JOURNAL OF GEOPHYSICAL RESEARCH, VOL. 101, NO. A7, PAGES 15,667–15,684, JULY 1, 1996

Interplanetary magnetic clouds, helicity conservation, and current-core flux-ropes

Ashok Kumar[1]

Department of Physics and Astronomy, The Johns Hopkins University, Baltimore, Maryland

D. M. Rust

Applied Physics Laboratory, The Johns Hopkins University, Laurel, Maryland

Abstract. A current-core flux-rope model for interplanetary magnetic clouds is presented which explains their average thermodynamic and magnetic properties. It is assumed that during a magnetic cloud's evolution, its total magnetic helicity, flux and mass are conserved and that the dynamics of a cloud is governed by the Lorentz self-force acting on its curved portions. Total magnetic energy and current in a magnetic cloud decrease monotonically as it elongates. Part of this magnetic energy is lost in overcoming solar gravity, part goes into the bulk kinetic energy, and the rest can be assumed to go into heating the plasma inside the cloud. Due to this dissipation of magnetic energy as heat, the temperature of an expanding cloud goes through a maximum before the cloud leaves the corona. The temperature may reach 1.7×10^6 K. As a cloud expands into interplanetary space, the total plasma beta asymptotically approaches a constant value between 0.39 and 0.52, irrespective of its initial value. Apart from explaining the heating and expansion of magnetic clouds, this model also provides expressions (scaling laws) for the magnetic field strength, temperature, radius, density, asymmetry of the magnetic field strength profile, slope of the plasma velocity profile inside clouds, and plasma beta, as functions of distance from the Sun. These theoretical results are compared with cloud data obtained between 0.3 and 4 AU from the Sun. The comparisons show a good agreement between observation and theory.

1. Introduction

A spacecraft observing the solar wind often encounters regions of enhanced magnetic field strength, called interplanetary magnetic clouds (IMCs), which show large and smooth variations in all field components [*Burlaga et al.*, 1981; *Klein and Burlaga*, 1982; *Burlaga et al.*, 1984; Burlaga, 1988]. The observed magnetic configuration in the IMCs is of a helical flux-rope and is reasonably consistent with cylindrically symmetric constant-α force-free solutions [*Burlaga*, 1988; *Lepping et al.*, 1990]. Earlier force-free models were considered by *Goldstein* [1983] and *Marubashi* [1986]. Field lines in IMCs apparently remain connected to the Sun, even beyond a few AUs, although clouds with links severed from the Sun are certainly imaginable. *Burlaga et al.* [1990] argue that a disconnected toroidal configuration [*Ivanov et al.*, 1989] is unlikely, however, since IMC signatures are not observed in pairs. *Farrugia et al.* [1991, 1993] related the slope of the velocity profile and the asymmetry of the magnetic strength profile inside clouds to their expansion. *Chen* [1989, 1990], *Chen and Garren* [1993], and *Garren and Chen* [1994] have modeled an IMC as a toroidally symmetric current loop which expands due to a Lorentz self-force acting on the curved portion of the loop. *Osherovich et al* . [1993a, 1993c, 1995] considered self-similar evolution of cylindrically symmetric flux-ropes under various conditions. The pressure and density obtained by a passing spacecraft at various locations in a magnetic cloud seem to be related by a polytropic relationship with an index of ~0.5 for electrons and ~1.2 for protons [*Osherovich et al.*, 1993b]. Interplanetary shock waves are often caused by fast moving IMCs, and their interaction with Earth's magnetosphere causes some of the largest geomagnetic storms observed.

Observations generally support the view that erupting filaments are the sources of IMCs [*Wilson and Hildner*, 1984, 1986; *Hundhausen*, 1988; *Rust*, 1994]. Statistical studies of coronal mass ejections (CMEs), of which IMCs form a subset, show them to be most commonly associated with filament eruptions [*Hundhausen*, 1988]. In a recent study, *Feynman and Hundhausen* [1994] argue that CMEs are associated with disturbances in magnetic structures in the solar atmosphere, which can cause destabilizations that, in turn, may or may not lead to flares or filament eruptions. *Rust and Kumar* [1994a] suggested that IMCs should be associated with erupting filaments, as they share a common helical flux-rope structure.

In this paper, we develop a current-core helical flux-rope model for IMCs to understand their evolution from the time they leave the Sun to the time, about 4 days later, that they reach Earth. We emphasize the global rather than the local aspects. We use globally conserved quantities to gain information about the evolution of various other quantities of interest. In this respect, our approach is complimentary to the MHD approach taken by *Osherovich et al.* [1993a, 1995] and

[1]Also at Applied Physics Laboratory, Johns Hopkins University, Laurel, Maryland.

Paper number 96JA00544.
0148-0227/96/96JA-00544$09.00

Chen [1989, 1990]. An important feature of our model is its use of the principle of conservation of magnetic helicity. This principle, first applied to explain the behavior of laboratory plasmas [*Taylor*, 1974], provides a powerful constraint on IMC models. In particular, conservation of magnetic helicity suggests that the magnetic energy stored in an expanding plasma should decrease with expansion. A heuristic justification for this can be obtained by realizing that, dimensionally, magnetic helicity is proportional to magnetic energy times a length scale, i.e., $H_m \propto (\text{length scale}) \times U_m$. Therefore as the length scales increase due to expansion, the magnetic energy must decrease to keep the magnetic helicity constant.

The plan of the paper is the following: We first develop the concept of a current-core flux-rope and apply it to a torus-shaped cloud. Next, we consider how an expanding flux-rope would evolve under the constraints of conservation of mass, magnetic flux, and magnetic helicity. We find that the magnetic energy decreases monotonically during the expansion and that 58% to 78% of this lost energy could possibly go into heating the IMC. This would explain the observed high temperatures of IMCs at 1 AU, which are otherwise very difficult to explain.

After discussing the dynamics and thermodynamics of IMCs, we consider other observable effects of expansion, namely, the variation of radius with distance from the Sun, asymmetry of the magnetic field, and the velocity profile inside a cloud. Finally, we compare the derived observables with data obtained from spacecraft between 0.3 and 4 AU from the Sun and briefly consider the implications of helicity conservation in flux-ropes in other astrophysical contexts.

2. Current-Core Flux-ropes

A magnetic cloud is usually modeled as a flux-rope with the cylindrically symmetric force-free Lundquist solution [*Burlaga et al.*, 1988; *Lundquist*, 1950] given by

$$\mathbf{B} = \hat{\mathbf{r}}\,0 + \hat{\boldsymbol{\theta}} B_0 J_1(\alpha \mu_0 r) + \hat{\mathbf{z}} B_0 J_0(\alpha \mu_0 r)\ . \tag{1}$$

Here α is the proportionality constant between current density and magnetic field $\mathbf{j} = \alpha \mathbf{B}$ and J_0 and J_1 are Bessel functions of first kind of order 0 and 1 respectively. The flux-rope length scale given by $(\alpha \mu_0)^{-1}$, which is the characteristic length scale for radial variations in the magnetic field.

The Lundquist solution has been used to describe relaxed states in laboratory pinch experiments [*Taylor*, 1974, 1986]. In these experiments, the plasma is necessarily confined within a conducting boundary situated at some fixed radius, and currents may be present right up to the boundary. The conducting boundary condition leads to determination of a set of discrete values for α. Therefore, in such situations all the relevant length scales, including the current confinement scale and the scale associated with $(\alpha \mu_0)^{-1}$ are dependent on the fixed boundary. Flux-ropes in astrophysical settings do not possess a fixed conducting boundary, and therefore the length scales involved need not depend upon conditions external to the flux-rope.

In the usual flux-rope models, the boundary of the flux-rope is taken to be where the total ambient pressure (magnetic pressure plus plasma pressure) balances the total pressure inside the flux-rope. Hence the length scale associated with the radial extent of the flux-rope again seems to depend upon conditions external to the flux-rope. However, strictly speaking, this pressure balance condition is valid only in those cases where the curvature of field lines can be neglected. When the field lines are strongly curved, as in the case of helical field lines (e.g., cylindrical force-free field) or in the case of circular field lines (e.g., curl-free field outside a cylindrical current-carrying region), then the magnetic tension of the field lines must be taken into account along with the magnetic pressure. In the particular cases mentioned above of force-free and curl-free configurations, the centrifugal force due to magnetic pressure of the field lines exactly balances the centripetal force due to tension in the inward curved field lines.

Helical flux-ropes are necessarily current carrying. One would expect that the currents flowing along a helical flux-rope must be confined within some finite radius beyond which a curl-free field with circular field lines would be present. We will specify this radius and other intrinsic length scales.

Consider a twisted flux-rope that locally looks like a cylindrical flux-rope and in which the magnetic field depends upon radius r only through the combination λr. Here λ^{-1} is the characteristic length scale for radial variations in the magnetic field. A second length scale of interest is the radius r_0 within which the axial current is confined, because twisted flux-ropes are necessarily current-carrying. The core current creates a surrounding curl-free field that drops steadily as one moves away from the flux-rope axis.

We can also consider a radius $r_1 > r_0$, where environmental influences become prominent. Changes in environmental conditions would influence the magnetic field, for example, outside r_1, but λ^{-1}, r_0 and l where l is the length of the flux-rope, would remain relatively unaffected.

Now we introduce the concept of a current-core flux-rope, in which the three length scales λ^{-1}, r_0, and l, representing radial variations in magnetic field, current confinement, and length of the flux-rope, respectively, are insensitive to changes in the environment and therefore are called intrinsic scales. We will show that, for a current-core flux-rope undergoing a quasi-static change in length while flux and magnetic helicity are conserved, the three length scales change in proportion:

$$\lambda^{-1} \sim r_0 \sim l\ . \tag{2}$$

In other words, a current-core flux-rope evolves self-similarly. During quasi-static evolution, the parameters λ, r_0 , and axial magnetic field strength B_0, will depend on l, but the functional form of the fields will be invariant .

Let us assume that the magnetic field and the vector potential take the following form:

For $r \le r_0(l)$

$$\begin{aligned} \mathbf{B}(r;l) &= B_0(l)\,\mathbf{b}^{\text{in}}(\lambda(l) r), \\ \mathbf{A}(r;l) &= \frac{B_0(l)}{\lambda(l)}\,\mathbf{a}^{\text{in}}(\lambda(l) r), \end{aligned} \tag{3}$$

where $B_0(l) = |\mathbf{B}(0;l)|$ and $\mathbf{b}^{\text{in}}$ and $\mathbf{a}^{\text{in}}$ are some dimensionless vector functions that satisfy $\nabla_x \times \mathbf{a}(x) = \mathbf{b}(x)$. The curl is taken with a dimensionless radial variable $x = \lambda r$. We have also used the fact that the vector potential scales with length l as $B_0(l)/\lambda(l)$. Similarly,

For $r \ge r_0(l)$

$$\mathbf{B}(r;l) = B_0(l)\mathbf{b}^{\text{out}}(\lambda(l)r),$$
$$\mathbf{A}(r;l) = \frac{B_0(l)}{\lambda(l)}\mathbf{a}^{\text{out}}(\lambda(l)r), \tag{4}$$

Conservation of axial flux ψ_z gives

$$\psi_z = \int_{r=0}^{r_0(l)} B_0(l) b_z^{\text{in}}(\lambda(l)r) 2\pi r\, dr$$
$$= \frac{B_0(l)}{\lambda^2(l)} f_1(\lambda(l)r_0(l)) = \text{const.} \tag{5}$$

Conservation of azimuthal flux ψ_θ gives

$$\psi_\theta = \int_{r=0}^{r_0(l)} \int_{z=0}^{l} B_0(l) b_\theta^{\text{in}}(\lambda(l)r)\, dr\, dz$$
$$= \frac{B_0(l)l}{\lambda(l)} f_2(\lambda(l)r_0(l)) = \text{const.} \tag{6}$$

Conservation of magnetic helicity $H_m = \oint_V \mathbf{A}\bullet\mathbf{B}\,dV$ gives

$$H_m = \frac{(B_0(l))^2 l}{(\lambda(l))^3} f_3(\lambda(l)r_0(l)) = \text{const.} \tag{7}$$

Where f_1, f_2, and f_3 are some functions of $\lambda(l)r_0(l)$ obtained after the integrations. From (5), (6), and (7) we obtain

$$\frac{\psi_z\psi_\theta}{H_m} = \frac{f_1(\lambda(l)r_0(l))f_2(\lambda(l)r_0(l))}{f_3(\lambda(l)r_0(l))}$$
$$\equiv f_4(\lambda(l)r_0(l)) = \text{const.} \tag{8}$$

In general, f_4 is not a constant function of its argument, therefore it can remain constant only if its argument remains constant, i.e.,

$$\lambda(l)r_0(l) = \text{const.} \tag{9}$$

From (5) and (9) we obtain

$$B_0(l) \sim (\lambda(l))^2 \sim (r_0(l))^{-2}. \tag{10}$$

From (6), (9), and (10) we finally get what we set out to show

$$(\lambda(l))^{-1} \sim r_0(l) \sim l, \tag{11}$$

i.e., the three relevant length scales are proportional to each other; therefore a current-core flux-rope evolves self-similarly. A cylindrically symmetric current-core flux-rope model for solar filaments was presented by Rust and Kumar [1994a]. Below we construct a toroidally symmetric current-core flux-rope model of IMCs.

3. Magnetic Cloud as a Toroidal Flux-rope

Locally, IMCs appear cylindrically symmetric, but if they connect back to the Sun, then globally, their structure should be closer to a torus with tapering ends (Figure 1). *Burlaga et al.* [1990], using data obtained on the same cloud from four spacecraft, argued in favor of such a configuration. (Other authors have advocated spheroidal or disconnected toroidal geometries [*Ivanov and Harshiladze*, 1985; *Ivanov et al.*, 1989; *Vandas et al.*, 1993].) The cylindrically symmetric

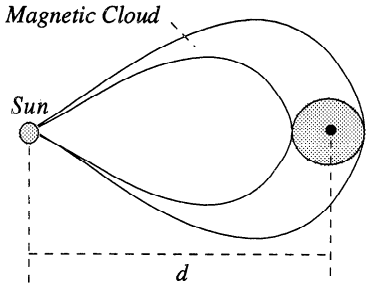

Figure 1. Expected shape of a magnetic cloud.

model then is only a first-order description. For a second-order description an IMC should be modeled as a large-aspect-ratio toroidally symmetric current-core flux-rope that remains connected to the Sun.

Chen [1989, 1990] and *Chen and Garren* [1993] developed a dynamical model of IMCs as toroidal flux-ropes that remain connected to the Sun. They included Lorentz stresses, pressure gradient forces, and the drag of the ambient medium in their force balance equation. They also assumed that no internal current dissipation takes place and that the equation of state is given by a polytropic law. With a polytropic index of 5/3 (adiabatic expansion), they obtained temperatures at 1 AU of a few kelvins, while the observed temperatures are tens of thousands of kelvins. Except for the temperature, most other properties of IMCs computed with their model are in reasonably good agreement with observations.

By assuming global conservation of magnetic helicity, flux, and mass in IMCs, we find a good fit to IMC observables, including temperature. We start with a model having as few parameters as possible to explain the average observed properties of IMCs. The use of global conservation laws will allow us to express observable quantities in terms of the distance of the apex of the flux-rope from the Sun. No dynamical considerations are necessary to obtain these scaling laws. In comparing derived physical quantities with observations, we assume that an average over many clouds' properties can be substituted for the properties of an average cloud. This is necessary, since data on the behavior with time of a single IMC are virtually nonexistent. Extant data describe many IMCs observed by various spacecraft located at different distances from the Sun. We assume these data correctly describe the properties of an average IMC as a function of distance from the Sun. Nevertheless, we do consider the dynamics in section 5.

Note that global conservation of magnetic flux and mass can also be incorporated in a theory in a local form by converting the integral forms of conservation equations into their differential forms. But the same cannot be done with magnetic helicity, which is a truly global (topological) quantity. This is evident from the explicit appearance of the vector potential in the integral expression for magnetic helicity, so that the helicity can be made gauge independent only by ensuring the appropriate boundary conditions [*Berger and Field*, 1984]. This dependence on boundary conditions is what makes magnetic helicity a global topological quantity.

Magnetic helicity essentially measures the linkages of field lines. Whether any two field lines are linked globally, or not, can be determined unambiguously, but it is not possible to say where the link is located. Thus helicity conservation can be used unambiguously only in the global sense. For conditions

under which a local magnetic helicity density can be defined, see *Berger and Field* [1984].

We model an IMC as a large-aspect-ratio toroidally symmetric current-core flux-rope with constant cross section. We assume that it remains connected to the Sun and that, inside, the current flows approximately parallel to the magnetic field so that the Lundquist solution [*Lundquist*, 1950] obtained from the condition $\mathbf{j}=\alpha\mathbf{B}$ is approximately applicable. Use of the Lundquist solution does not mean that clouds are "force-free" with vanishing Lorentz stresses $\mathbf{j}\times\mathbf{B}$. Lorentz stresses are needed to explain the expansion of clouds. In section 5, on dynamics, we will show explicitly that an angle of 3-4° between the currents and the fields inside a cloud can provide the necessary force to drive a cloud's expansion. However in the model, we assume that the currents and fields are approximately parallel, and we use the Lundquist solution even though the currents and fields are so large that even a small angle between them is enough to drive the expansion of the cloud.

Osherovich et al. [1993a] showed that a cylindrically symmetric low-beta force-free flux-rope cannot expand radially. It can only undergo radial oscillations. With a finite beta, radial expansion becomes possible [*Osherovich et al.*, 1995], and if the flux-rope is curved, it experiences the so-called Lorentz self-force [*Chen*, 1989; *Chen and Garren*, 1993; *Garren and Chen*, 1994; *Shafranov*, 1966; *Landau and Lifshitz*, 1960].

Assume that currents flow approximately parallel to fields inside the cloud and that a current-free solution holds outside:

$$\mathbf{j}=\frac{1}{\mu_0}\nabla\times\mathbf{B}=\alpha\mathbf{B} \quad r\le r_0, \tag{12}$$

$$\mathbf{j}=\frac{1}{\mu_0}\nabla\times\mathbf{B}=\mathbf{0} \quad r>r_0, \tag{13}$$

where we are using toroidally distorted cylindrical coordinates (r,θ,z) with z along the toroidal axis of the torus (Figure 2).

The curl-free field outside the boundary is similar to the field due to a current-carrying ring, and it has no z component. In the absence of current sheets at the boundary, the field components are continuous, and we obtain a boundary condition for the internal fields as $B_z=0$ at the boundary. We take the cylindrically symmetric Lundquist solution to be valid in the interior, and for the exterior we use the solution for a current-carrying ring. This simplification is valid only for large-aspect-ratio torii ($l/r_0>>1$). Exact solutions for these equations in toroidal geometries are not available. For a second-order generalization of the Lundquist solution in toroidal geometry, see *Miller and Turner* [1981].

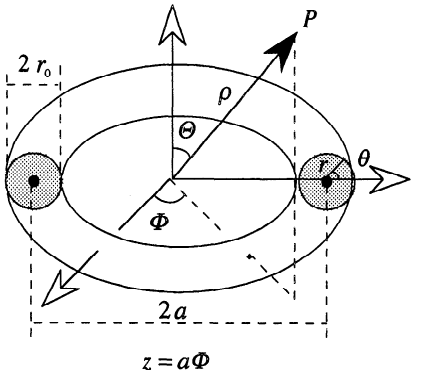

Figure 2. Magnetic cloud modeled as a torus.

3.1. Interior Solution

For $r\le r_0$ we get

$$\mathbf{B}=B_0\left(\hat{\mathbf{r}}0+\hat{\boldsymbol{\theta}}HJ_1(\alpha\mu_0 r)+\hat{\mathbf{z}}J_0(\alpha\mu_0 r)\right), \tag{14}$$

where J_0 and J_1 are Bessel functions of order 0 and 1 respectively and $H=\pm1$ determines the handedness (chirality) of helical field lines. This is basically the Lundquist solution. In the following we will assume $H=+1$.

The condition that the z component of the field goes to zero at the current confinement boundary gives

$$J_0(\alpha\mu_0 r_0)=0. \tag{15}$$

This restricts the values of $\alpha\mu_0 r_0$ to be one of the zeroes of J_0, i.e.,

$$r_0=x_0(\alpha\mu_0)^{-1} \tag{16}$$

where x_0 is a zero of J_0. We find that r_0 is linearly related to the length scale $(\alpha\mu_0)^{-1}$ with a dimensionless multiplicative constant x_0. This is just (9) in a different form. In terms of the dimensionless radial variable $x\equiv\alpha\mu_0 r$, we can write the field as

$$\mathbf{B}=B_0\left(\hat{\mathbf{r}}0+\hat{\boldsymbol{\theta}}J_1(x)+\hat{\mathbf{z}}J_0(x)\right) \quad x\le x_0. \tag{17}$$

The total axial flux of the flux-rope is given by

$$\psi_z=\int_0^{r_0}B_z(\alpha\mu_0 r)2\pi r\,dr=\frac{2\pi B_0}{(\alpha\mu_0)^2}\int_0^{x_0}J_0(x)x\,dx. \tag{18}$$

If now the flux-rope were to undergo a quasi-static homogeneous deformation, then B_0, r_0, and α would change, but the dimensionless number x_0, being a zero of J_0, is not going to change. Therefore the integral on the right-hand side evaluates to a dimensionless constant k_1,

$$\psi_z=\frac{2\pi B_0}{(\alpha\mu_0)^2}k_1. \tag{19}$$

Similarly, the total z current is

$$I_z=\frac{2\pi B_0}{\alpha\mu_0^2}k_1. \tag{20}$$

The vector potential inside the boundary can be taken as

$$\mathbf{A}=\frac{\mathbf{B}}{\alpha\mu_0}. \tag{21}$$

3.2. Exterior Solution

The field outside the boundary is curl-free. It is due to a ring current flowing along the torus. The vector potential for this external field can be written as

$$\mathbf{A}=\hat{\boldsymbol{\rho}}\frac{B_\rho}{\alpha\mu_0}+\hat{\boldsymbol{\Theta}}\frac{B_\Theta}{\alpha\mu_0}+\hat{\boldsymbol{\Phi}}(A_\Phi-q). \tag{22}$$

Here spherical coordinates (ρ,Θ,Φ) are being used with the geometry shown in Figure 2, and all quantities depend upon ρ and Θ only. We have

$$A_\Phi = \frac{2B_0 k_1}{\alpha \mu_0}\frac{a}{k^2}\frac{\left[\left(2-k^2\right)K(k)-2E(k)\right]}{\sqrt{a^2+\rho^2+2a\rho\sin\Theta}}, \qquad (23)$$

where

$$k^2 = \frac{4a\rho\sin\Theta}{a^2+\rho^2+2a\rho\sin\Theta} \qquad (24)$$

and

$$q = \frac{k_1}{\alpha\mu_0}\left[\ln\left(\frac{8a}{b}\right)-2\right]. \qquad (25)$$

$K(k)$ and $E(k)$ are complete elliptic integrals of the first and second kind, respectively, and k_1 is the dimensionless constant encountered earlier. The magnetic field is

$$\mathbf{B} = \left(\hat{\boldsymbol{\rho}}\frac{1}{\rho\sin\Theta}\frac{\partial(\sin\Theta A_\Phi)}{\partial\Theta} - \hat{\boldsymbol{\Theta}}\frac{1}{\rho}\frac{\partial(\rho A_\phi)}{\partial\rho} + \hat{\boldsymbol{\Phi}}0\right). \qquad (26)$$

It can be shown that in the limiting case of a large-aspect-ratio toroidal flux-rope, the components of the magnetic field and the vector potential are continuous across the boundary. The continuity holds only in the limit of large aspect ratio. To facilitate the algebra it is helpful to use Landen's transformation [*Lamb*, 1993], pp. 237-240] to change variables from (ρ,Θ) to (r_1,r_2) (see Figure 3). For a large-aspect-ratio torus, the boundary of the torus is approached for $r_2 >> r_1$, and the variable r_1 takes up the role of radius in the toroidally curved cylindrical coordinates used to describe fields within the boundary.

The total magnetic energy of the flux-rope is given by

$$U_m = \frac{1}{2\mu_0}\int|\mathbf{B}|^2 dV = \frac{\pi l B_0^2}{\alpha^2\mu_0^3}k_1^2\left(\ln\left(\frac{8a}{r_0}\right)-1\right), \qquad (27)$$

where k_1 is a dimensionless constant described earlier and $l = 2\pi a$ is the length of the torus. The magnetic helicity of the toroidal current-core flux-rope is given by

$$H_m = \int \mathbf{A}\bullet\mathbf{B}\,dV = \frac{1}{(\alpha\mu_0)}\int|\mathbf{B}|^2 dV = \frac{2}{\alpha}U_m. \qquad (28a)$$

These formulas for magnetic energy and helicity are approximate and are valid only in the limit of large aspect ratio. Using (16) we can write the last equality in (28a) as:

$$H_m = \left(\frac{\mu_0}{x_0}\right)r_0 U_m \qquad (28b)$$

i.e.,

$$H_m \propto r_0 U_m \qquad (28c)$$

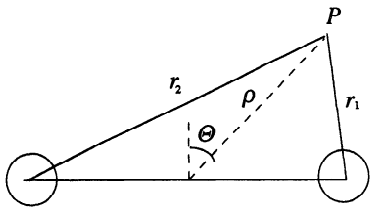

Figure 3. Geometry of Landen's transformation.

where $x_0 \cong 2.405$ is the first zero of J_0. (28b) and (28c) give, within a constant factor, the magnetic helicity of the toroidal flux-rope in terms of the radius of the flux-rope and its magnetic energy. This is a concrete example of the point made in the introduction that magnetic helicity is proportional to the product of a length scale and the magnetic energy, viz., $H_m \propto (\text{length scale})\times U_m$. Therefore, as the flux-rope expands, its magnetic energy must decrease to keep the magnetic helicity constant. Later we will argue that part of this lost magnetic energy goes into internal heating.

Using (28), (27), (19) and (16), we can write the magnetic helicity as

$$H_m \propto \psi_z{}^2\frac{l}{r_0}\left(\ln\left(\frac{l}{r_0}\right)+\text{constant}\right). \qquad (29)$$

Conservation of axial flux and helicity during a quasi-static change in length l of the flux-rope implies that the ratios l/r_0 and a/r_0, do not depend upon l. Inclusion of conservation of azimuthal flux gives a condition similar to Equation (9). Therefore, we will not use conservation of azimuthal flux for the following. Then, energy and magnetic helicity can be written as

$$U_m = \frac{\pi l B_0^2}{\alpha^2\mu_0^3}k_2, \qquad (30)$$

and

$$H_m = \frac{2\pi l B_0^2}{(\alpha\mu_0)^3}k_2. \qquad (31)$$

Equations (16), (19), (20), (30), and (31) are the main results we will use in this paper. We will treat k_1 and k_2, which are dimensionless constants for current-core flux-ropes, as unchanging with time.

4. Expanding Current-Core Flux-rope

The current-core flux-rope described in the previous section has only three independent magnetic parameters: strength of the axial field B_0, the parameter α, and the length l. The cross-sectional radius, r_0, of the current carrying part is given in terms of α as $x_0(\alpha\mu_0)^{-1}$, where x_0 is a zero of Bessel function J_0. To determine the state of the flux-rope as a function of its length, we need impose only conservation of axial magnetic flux, conservation of total magnetic helicity, and conservation of mass. Conservation of azimuthal flux gives a relation similar to (9), which we already have in (16). For the simple flux-rope model for the magnetic clouds considered in this paper, $\alpha\mu_0 r_0$ becomes equal to a zero of Bessel function J_0 due to continuity of the axial component. This condition is more precise than the condition obtained from including the azimuthal flux conservation which gives the condition that $\alpha\mu_0 r_0$ be a constant during the evolution.

The model of *Chen* [1989] and *Chen and Garren* [1993] also conserved axial and azimuthal flux. The scaling laws obtained with these models would have same asymptotic form as ours if one were to use just axial and azimuthal flux conservation or axial flux conservation along with helicity conservation. In the case of laboratory experiments on relaxation in toroidal pinch plasmas, the two invariants most often chosen are magnetic helicity and axial flux [*Taylor*, 1986]. When a plasma is confined by a conducting surface, the magnetic

helicity H_m of a toroidal pinch is given by the product of the axial and azimuthal fluxes ψ_z and ψ_θ as $H_m \sim \psi_z \psi_\theta$. Therefore the conservation of any two of theses quantities implies conservation of the third. This might seem to imply that conservation of helicity does not give anything new. But in the general case, magnetic helicity proves to be a better invariant than the fluxes. Equation (28), showing that energy decreases with expansion while helicity is conserved, remains valid even in cases where flux conservation cannot be used. For example, in a spherical volume only magnetic helicity remains a good invariant (see the discussion following equation (6.1) in the article by *Taylor* [1986]).

Since conservation of magnetic helicity can be used even in cases where flux conservation cannot, we will focus on the relationship linking magnetic energy and cloud size through magnetic helicity, even though for the particular model considered in this paper, we might as well have used fluxes.

4.1. Conservation of Magnetic Flux

Large-scale magnetic fields in a plasma with high electrical conductivity are said to be frozen-in. In our case, this means that the magnetic flux along the axis of a cloud remains constant over time. If the starting length of the toroidal flux-rope is taken to be l_0, then using (19), the flux at a different length l is given by

$$\frac{2\pi B_0(l)}{\left(\alpha(l)\mu_0\right)^2}k_1 = \frac{2\pi B_0(l_0)}{\left(\alpha(l_0)\mu_0\right)^2}k_1 = \text{const.} \tag{32}$$

Therefore

$$\frac{B_0(l)}{\alpha(l)^2} = \frac{B_0(l_0)}{\alpha(l_0)^2}. \tag{33}$$

4.2. Conservation of Magnetic Helicity

Elsasser [1956] and *Woltjer* [1958] showed that magnetic helicity

$$H_m = \int_V \mathbf{A}\bullet\mathbf{B}dV \tag{34}$$

is conserved in ideal MHD. However, since field lines do not reconnect in ideal MHD, infinitely many other invariants related to the helicity of individual field lines are possible. *Taylor* [1974, 1986] conjectured that in the presence of some resistivity, out of all ideal MHD magnetic helicity invariants, only the total magnetic helicity would remain approximately constant, i.e. magnetic helicity is a robust invariant of MHD [*Ruzmaikin and Akhmetiev*, 1994]. If field lines cross a boundary of the system, then a more appropriate gauge-invariant helicity integral must be used [*Berger and Field*, 1984; *Jensen and Chu*, 1984; *Finn and Antonsen*, 1985]. However in our model, the helicity integral is evaluated over the whole torus, and (34) is sufficient.

Berger [1984], using Schwarz's inequality, obtained rigorous limits on magnetic helicity dissipation. Equation (25) of Berger's paper is written below in SI units.

$$\Delta H \le 2\mu_0\sqrt{\overline{\eta}\left(U_i^2 - U_f^2\right)\Delta t}, \tag{35}$$

where $\eta = \left(\mu_0\sigma\right)^{-1}$, σ is conductivity, U stands for energy, and subscripts i and f denote initial and final, respectively. Δt is the time interval during which energy and helicity dissipation are considered. We take this interval to be 4 days. Using $H_i = \left(2/\alpha_i\right)U_i$ and noting that most IMCs originate in filament eruptions, we take $0.006 \le \alpha_i \le 0.06\ \mathrm{A\,m^{-2}\,T^{-1}}$ for filaments [*Rust and Kumar*, 1994a]. For conductivity we use the SI form of the expression given by *Sturrock* [1994], which gives $\sigma = 6\times10^{-5}T^{3/2}\ \mathrm{ohm^{-1}\,m^{-1}}$. Assuming on average $T \cong 10^5\ \mathrm{K}$, we obtain

$$\frac{\Delta H}{H_i} \le 0.001. \tag{36}$$

Therefore, less than one tenth of a percent of the magnetic helicity is lost during a cloud's passage from the Sun to Earth. We conclude that, in the absence of any exchanges with the Sun, the magnetic helicity of a cloud remains constant to a very good approximation. On the other hand, we will find that the magnetic energy dissipates with time, probably due to small-scale turbulence. We will conclude that, at small scales, an anomalous turbulent conductivity much smaller than the ideal conductivity might be present.

Anomalous conductivity could possibly change the magnetic helicity spectrum in IMCs. *Frisch et al.* [1975], *Matthaeus and Goldstein* [1982], *Matthaeus et al.* [1982] and *Matthaeus and Montgomery* [1980] have argued that in the presence of MHD turbulence, an inverse cascade of magnetic helicity might exist: as magnetic energy is transferred to smaller and smaller scales, where dissipation is much more efficient, magnetic helicity might be transferred to larger and larger scales, where dissipation is inefficient. For discussion of magnetic helicity in MHD turbulence with or without a mean magnetic field present, see *Matthaeus and Goldstein* [1982], *Stribling et al.* [1994], and *Ghosh et al.* [1995]. We conclude that magnetic helicity might be approximately conserved even in the presence of turbulence while magnetic energy is efficiently dissipated. We assume that the magnetic helicity in IMCs is conserved to a high degree.

4.3. Effect of Elongation: The Scaling Laws

With l_0 as the initial length of the flux-rope and l as the length at a subsequent time, using Equation (31), we get for magnetic helicity

$$\frac{2\pi B_0(l)^2 l}{\left(\alpha(l)\mu_0\right)^3}k_2 = \frac{2\pi B_0(l_0)^2 l_0}{\left(\alpha(l_0)\mu_0\right)^3}k_2 = \text{const.} \tag{37}$$

Then, from (33) and (37), we get

$$B_0(l) = B_0(l_0)\left(\frac{l_0^2}{l^2}\right), \tag{38}$$

and

$$\alpha(l) = \alpha(l_0)\left(\frac{l_0}{l}\right). \tag{39}$$

From (16) and (39) we obtain for the minor radius

$$r_0(l) = r_0(l_0)\left(\frac{l}{l_0}\right), \tag{40}$$

and using

$$2\pi a(l) = l \tag{41}$$

we obtain for the major radius

$$a(l) = a(l_0)\left(\frac{l}{l_0}\right). \quad (42)$$

For the total z current and total magnetic energy we use (20), (30), (38) and (39) to obtain

$$I_z(l) = I_z(l_0)\left(\frac{l_0}{l}\right), \quad (43)$$

and

$$U_m(l) = U_m(l_0)\left(\frac{l_0}{l}\right). \quad (44)$$

Using conservation of mass we get

$$V(l) = V(l_0)\left(\frac{l^3}{l_0^3}\right), \quad (45)$$

and

$$n(l) = n(l_0)\left(\frac{l_0^3}{l^3}\right), \quad (46)$$

where $V = \pi r_0^2 l$ is the total volume and n is the number density. Thermodynamic quantities are assumed to be averaged over the volume of the flux-rope.

Many authors have given similar scaling laws, with identical or different exponents, for the various quantities discussed above. In particular, *Osherovich et al.* [1993c] used a self-similar radial expansion for a cylindrically symmetric MHD polytrope to obtain the field strength at the axis as $B_0 \sim d^{-1/\gamma}$, where d is the distance from the Sun and γ is the polytropic index. *Osherovich et al.* [1993a] argued that the electron polytropic index, defined by them as the ratio of the logarithm of the electron pressure to the logarithm of the electron density measured at different points inside a cloud, tends to be less than 1 inside the cloud and is typically close to 1/2. For $\gamma = 1/2$ the scaling law of *Osherovich et al.* [1993c] for axial field strength is identical to ours.

In section 2 it was shown that the three intrinsic length scales associated with a flux-rope evolve in proportion. To obtain this self-similar evolution, we used conservation of axial flux, azimuthal flux, and magnetic helicity. In a flux-rope model for which one of the three length scales is fixed a priori (possibly in terms of the other two length scales), then conservation of axial and azimuthal fluxes only might be sufficient to define its evolution. However in the general case one would need conservation of magnetic helicity. In our model based on the Lundquist solution we argued that the current confinement radius occurs at the first zero of the Bessel function J_0. Actually, one does not require this to obtain the scaling laws. Had we assumed that the current confinement occurs within an arbitrary radius not necessarily equal to the zero of J_0, we would still have obtained the same scaling laws, provided that conservation of magnetic helicity and of the fluxes were invoked. But conservation of flux alone does not give enough constraints to obtain the scaling laws in this more general case.

4.4. Dissipation of Magnetic Energy

Total current I_z and total magnetic energy U_m in our model decrease inversely with length. Magnetic energy decrease in solar filament eruptions has been discussed by *Moore* [1988]. We emphasize that the conservation of magnetic helicity requires that the magnetic energy of an expanding flux-rope must decrease with its expansion. Since, by assumption, no energy is input from the Sun during the expansion, the lost magnetic energy must appear in some other form. The principle of helicity conservation does not tell us what forms this lost energy might take. If magnetic forces are responsible for driving the cloud's motion, then some of the magnetic energy goes into overcoming solar gravity and some goes into providing the bulk kinetic energy of motion. For simplicity, we assume that other losses such as due to creation shocks, accelerating particles, and drag of the ambient medium, are negligible and that the rest of the available magnetic energy goes into heating the plasma in the cloud. This heating can be thought of as being due to an anomalous resistivity. For the following development, we only need to know that the magnetic energy decreases with increasing flux-rope length. Knowledge of the exact mechanism of energy dissipation is not necessary; nevertheless, a few comments on the energy dissipation mechanism are in order.

Lepping et al. [1991] used the method of *Matthaeus et al.* [1982] and *Matthaeus and Goldstein* [1982] to obtain power spectra and helicity spectra of the magnetic field within a large magnetic cloud [see also *Burlaga et al.* 1985]. They found that all spectra show a strong wavenumber dependence of $\kappa^{-5/3}$, especially toward the large wavenumber range, over more than two decades. This is a characteristic of fully developed inertial-range turbulence [*Kolmogorov*, 1941, 1962; *Kraichnan*, 1965; *Batchelor*, 1970]. Even though the amount of turbulence present at 1 AU is small, it might be a relic of much stronger turbulence present during earlier phases of a cloud's life as a violently erupting filament. *Vainshtein et al.* [1993] mention that turbulent dissipation of the magnetic field follows a chaotic arrangement of current sheets and proceeds at a time-scale of several turnover times of a vortex. The turnover time is the ratio of the size of the vortex to the velocity. It is the shortest time-scale available. On the other hand, laminar dissipation has a time-scale of the square root of the magnetic Reynolds number times the turnover time, which is much longer than the turbulent dissipation time-scale. Therefore turbulent dissipation in IMCs must be much more efficient than laminar dissipation.

Large-scale (small wavenumber) Fourier components of magnetic fields in astronomical settings are preserved due to low resistivity. However under continuous deformations that maintain a quasi-static equilibrium, magnetic stresses will spontaneously create small-scale (large wavenumber) discontinuities in the field throughout the volume for almost all field topologies [*Parker*, 1994]. Current sheets form with these discontinuities, and rapid reconnections take place on small scales. The large-scale quasi-static equilibrium throughout the volume is not significantly disturbed.

In light of the above, we can say that even though the large-scale structure of an IMC may be explained reasonably well with a constant-α force-free model with no field discontinuities or current sheets, at smaller scales discontinuities and current sheets could cause magnetic energy and net current to decrease with time. Their dissipation could heat the cloud, as argued below.

5. Dynamics

5.1. Lorentz Self-Force

Many authors have addressed the question of what propels magnetic clouds (and the solar wind in general), but this question has not yet been fully answered. In flux-ropes carrying a net current, the so-called Lorentz self-force can act on curved portions [*Mouschovias and Poland*, 1978; *Anzer*, 1978; *Chen*, 1989; *Chen and Garren*, 1993]. *Garren and Chen* [1994] studied the Lorentz self-force on a curved current loop of arbitrary shape. They found that the self-force is strongest where the radius of curvature is smallest and that the self-force acting on a small portion of the flux-rope could be approximated by the self-force on a torus-shaped current loop with the condition that the major radius of the torus be equal to the local radius of curvature. In the following, we will consider the influence of the Lorentz self-force on the dynamics of magnetic clouds in more detail.

From (20) and (27), the total magnetic energy stored in the toroidal flux-rope described in the previous section is given by

$$U_m = \frac{\mu_0}{2} I_z^2 a \left(\ln\left(\frac{8a}{r_0}\right) - 1 \right). \tag{47}$$

Therefore, the effective self-inductance is

$$L = \mu_0 a \left(\ln\left(\frac{8a}{r_0}\right) - 1 \right). \tag{48}$$

The Lorentz self-force per unit length acting radially outward along the major radius is [see also *Garren and Chen*, 1994; *Shafranov* , 1966; *Landau and Lifshitz* 1960])

$$f_L = \frac{I_z^2}{4\pi a}\frac{\partial L}{\partial a} = \frac{\mu_0}{4\pi}\frac{I_z^2}{a}\left(\ln\left(\frac{8a}{r_0}\right) - 1 \right) = \frac{U_m}{2\pi a^2}, \tag{49}$$

where use has been made of the fact derived earlier that the ratio of major radius to minor radius remains constant. Using (44) and (49), we can write the self-force per unit length in terms of initial magnetic energy U_{m0} and initial major radius a_0 as

$$f_L = U_{m0}\frac{a_0}{2\pi a^3} \tag{50}$$

5.2. Lorentz Self-Force and the Lundquist Solution

To describe the magnetic field structure inside a cloud, we relied on the Lundquist solution, for which all Lorentz stresses vanish ($\mathbf{j}\times\mathbf{B}=\mathbf{0}$). But on the other hand, to describe the dynamics of the magnetic cloud, we used the Lorentz self-force. That implies that the Lorentz stresses do not vanish. This apparent contradiction can be resolved by looking at the conditions for approximate validity of the Lundquist solution. The Lundquist solution was derived for the case in which the current density is parallel to the magnetic field ($\mathbf{j}=\alpha\mathbf{B}$), which incidentally also implies the vanishing of the Lorentz stresses. The Lundquist solution would still remain approximately valid if the current density and the magnetic field vectors were to make a small angle χ with respect to each other. However, if the current density and magnetic field are both strong, then even a small angle between them can give rise to significant Lorentz stresses. In the case of solar filaments, *Rust and Kumar* [1994a] showed that a χ lying between 0.36° degrees and 3.6° degrees is enough to support the dense filament material against solar gravity. Therefore, the Lundquist solution remains approximately valid even in some non-force-free cases.

In a large-aspect-ratio toroidal flux-rope, even a small angle χ between the current density and the magnetic field is sufficient to provide the needed Lorentz self-force. Using (50) and (16) and $|\mathbf{j}\times\mathbf{B}| = |\mathbf{j}||\mathbf{B}|\sin(\chi)$, we see that

$$\sin(\chi) \cong \frac{\pi}{x_0}\left(\frac{r_0}{l}\right), \tag{51}$$

where $x_0 \cong 2.405$ is the first zero of the Bessel function J_0. For a large-aspect-ratio torus we have $(r_0/l) << 1$ which implies $\chi << 1$. For a typical magnetic cloud radius of 0.15 AU at 1 AU, we get $\chi \cong 3.6°$, which is quite small.

5.3. Dynamical Model

An isolated toroidal current-carrying flux-rope will experience a radially outward Lorentz self-force (Figure 4). If any inward acting forces present are unable to balance the self-force, then the loop will expand radially while the center of mass remains stationary. In IMCs the center of mass evidently experiences a force. Therefore the cloud dynamics is more complicated than that in isolated toroidal current loops in which the Lorentz self-force acts radially outward in all directions.

Figure 5 shows a realistic geometry for an expanding flux-rope near the Sun. Near the photospheric footprints, the field lines are virtually straight. There is no Lorentz self-force acting in this part. Also due to the high density and high plasma beta of the photosphere, the submerged part of the flux-rope can be assumed to be dynamically unaffected by the Lorentz self-force. Therefore we need consider only the Lorentz self-force acting on the upper portions of the flux-rope.

In our dynamical flux-rope model (1) The global shape of the flux-rope is still assumed to be approximately that of a large-aspect-ratio torus, and (2) the total Lorentz self-force acting on the center of mass is given by integrating the vertical component of radially directed force f_L over the top portion of the flux-rope. The top portion can be described by an effective toroidal angle θ_0, as shown in Figure 5. We get, for the force acting on the center of mass,

$$F_{CM} = 2 f_L a \sin(\theta_0) \tag{52}$$

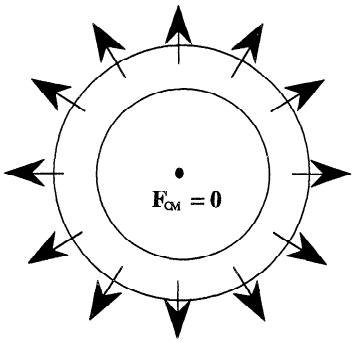

Figure 4. Lorentz self force on an isolated torus shaped flux-rope acts radially outwards such that the net force on the center of mass is zero.

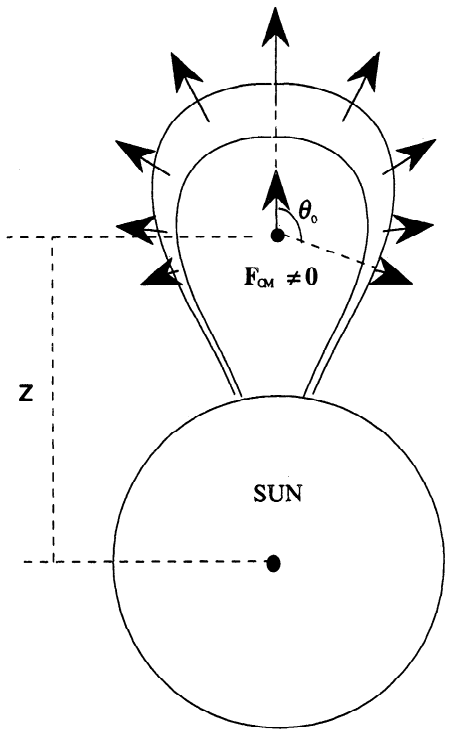

Figure 5. Lorentz self force on a solar flux-rope being ejected from the Sun. The force is maximum on the leading edge and is directed away from the Sun. Near the footpoints attached to the Sun the flux-rope appears to be virtually straight, which causes the Lorentz self force to vanish in the lower parts of the flux-rope. In this case the center of mass experiences a net force directed away from the Sun.

where a is the major radius. The case $\theta_0 = \pi$ corresponds to integrating over the whole flux-rope, and we see that F_{CM} vanishes in this case.

Now consider the motion of the center of mass M under the influence of gravity and the Lorentz self-force. Newton's second law gives

$$M\ddot{z}(t) = (1-s)U_{m0}\frac{a_0}{a(t)^2} - |U_{G0}|\frac{z_0}{z(t)^2}, \tag{53}$$

where

$$s \equiv 1 - \frac{\sin(\theta_0)}{\pi}. \tag{54}$$

Consequently, the limits on s are

$$\left(1-\frac{1}{\pi}\right) \le s \le 1 \tag{55}$$

or

$$s_{\max} \cong 1 \text{ and } s_{\min} \cong 0.68. \tag{56}$$

The initial gravitational potential energy is

$$U_{G0} = -G\frac{M_s M}{z_0} \tag{57}$$

and the distance of the center of mass from Sun center is

$$z(t) \cong R_s + a(t), \tag{58}$$

where M_s and R_s are the mass and radius of the Sun, respectively. Using the identity $(\dot{q})^2 = 2\int \ddot{q}\, dq$ and the initial condition $U^{KE}_{cm\,0} = 0$ we obtain the kinetic energy:

$$U^{KE}_{cm} = (1-s)U_{m0}\left(1-\frac{a_0}{a}\right) - |U_{G0}|\left(1-\frac{z_0}{z}\right). \tag{59}$$

The speed of the center of mass becomes

$$V_{cm} = V_{escape}\sqrt{\frac{1-s}{\beta_{G0}}\left(1-\frac{z_0-R_s}{z-R_s}\right) - \left(1-\frac{z_0}{z}\right)}, \tag{60}$$

where $V_{escape} \equiv 2GM_s/z_0$ is the escape speed. The initial gravitational beta $\beta_{G0} = |U_{G0}|/U_{m0}$ is the ratio of initial gravitational energy and initial magnetic energy of the flux-rope. Figure 6 shows the speed of the center of mass as a function of the distance from the Sun for various values of initial height. Consistent with observations, low-lying flux-ropes accelerate faster and have larger final speeds. In conjunction with equation (58), equation (53) can be thought of as a differential equation for temporal evolution of the major radius which can easily be solved numerically. Due to the self-similar expansion, the minor radius evolves in proportion to the major radius, and the time behavior of the minor radius can be determined. Far from the Sun ($z(t) >> R_s$), V_{cm} approaches a constant value and since $z(t) \cong a(t)$ holds, V_{cm} also becomes equal to the rate of change of the major radius with time. Therefore, far from the Sun the major radius and the minor radius of the toroidal cloud both evolve linearly with time. Closer to the Sun their evolution is more complicated.

From (59) we see that the kinetic energy of a rope's center of mass asymptotically reaches a constant value as distance from the Sun increases. The final kinetic energy attained at large distances from the Sun is

$$U^{KE}_{cm\,f} = (1-s)U_{m0} - |U_{G0}|, \tag{61}$$

and the final center of mass speed is

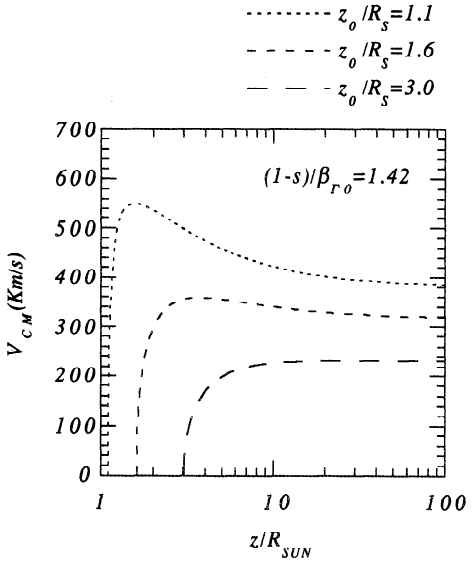

Figure 6. Speed of the center of mass of an erupting flux-rope as a function of the distance from the Sun for various values of the initial heights. Consistent with observations, the low lying flux-ropes accelerate faster and have larger final speeds.

$$V_{\mathrm{cm}\,f} = V_{\mathrm{escape}}\sqrt{\left[\frac{1-s}{\beta_{G0}} - 1\right]}. \tag{62}$$

Assuming the following typical values for the mass and final kinetic energy for an ejected magnetic cloud

$$M = 5\times10^{15}\,\mathrm{g}, \tag{63}$$

$$U^{\mathrm{KE}}_{\mathrm{cm}\,f} = 4\times10^{30}\,\mathrm{ergs} \tag{64}$$

we obtain

$$U_{G0} = 9.5\times10^{30}\,\mathrm{ergs}, \tag{65}$$

$$U_{m0} = \frac{\pi}{\sin(\theta_0)}\left(U^{\mathrm{KE}}_{\mathrm{cm}\,f} + U_{G0}\right) = \frac{4.24\times10^{31}}{\sin(\theta_0)}\,\mathrm{ergs}, \tag{66}$$

$$\beta_{G0} = 0.224\sin(\theta_0), \tag{67}$$

$$V_{\mathrm{cm}\,f} \cong 400\ \mathrm{km/s}, \tag{68}$$

$$V_{\mathrm{Front\,Edge}\,f} = 2V_{\mathrm{cm}\,f} \cong 800\ \mathrm{km/s}, \tag{69}$$

$$\frac{1-s}{\beta_{G0}} \cong 1.42. \tag{70}$$

Figure 6 shows a plot of V_{cm} versus distance from the Sun for various values of z_0 and with $(1-s)/\beta_{G0} = 1.42$.

Coming back to (61), we see that ultimately a fraction (1-s) of the magnetic energy goes into bulk kinetic energy of center of mass and into overcoming solar gravity. With a little algebra and using self-similarity of evolution, (all length scales change in proportion), it can further be shown that the kinetic energy of major radial expansion about the center of mass is same as the kinetic energy of center of mass, while the kinetic energy of the minor radial expansion is negligible for a large aspect ratio toroidal cloud. Therefore the total kinetic energy of a cloud is just twice its center of mass kinetic energy.

The remaining fraction h of the available energy, which we will call the deficit energy, can further be spent in accelerating high energy particles, in shocks, in overcoming drag of the ambient medium and in internal heating. It is difficult to estimate the partition of energy into these various sinks. However, taking into consideration the observed high temperatures in the clouds along with the availability of energy, it is hard to escape the conclusion that a significant part of this deficit energy goes into internal heating. For simplicity we will assume that all of the deficit energy goes into internal heating.

Independent of dynamical considerations, conservation of helicity gives us an expression for the magnetic energy decrease as a function of flux-rope size (28b). Solving a dynamical evolution equation with all the forces and dissipation mechanisms that may be present should, in principle, give the same result. However if one forgets to include a particular force or dissipation mechanism in the dynamical equations, then the equations are not going to sound a warning bell. They will simply give a certain rate of change in magnetic energy consistent with energy conservation and the effects of the included forces. However this rate of change will not be the correct one. To determine the correct rate of magnetic energy change short of knowing all the forces and their effects, one has to use some external criterion, which ordinarily would mean falling back on observations. Use of helicity conservation gives us such an external criterion.

In the magnetic cloud model by *Chen* [1989], mainly the Lorentz forces (especially the Lorentz self-force discussed in section 5) are responsible for acceleration. Therefore, in that model, the magnetic energy goes into kinetic energy and into losses due to the drag of ambient medium. Assuming, instead, that the lost magnetic energy appears as gain in thermal energy in the cloud along with gain in total kinetic energy and gravitational potential energy, we can use energy conservation to obtain the magnetic energy dissipated as heat dQ,

$$0 = dQ + dU_m + dU_G + dU_{\mathrm{KE}}. \tag{71}$$

Note that the total kinetic energy includes the kinetic energy of the center of mass and the kinetic energy of major and minor radial expansion. As mentioned earlier, this total kinetic energy is approximately equal to twice the center of mass kinetic energy for a large aspect ratio cloud. Substituting for all the quantities we obtain

$$dQ = -(2s - 1 - \beta_G)\,dU_m \equiv -h\,dU_m, \tag{72a}$$

where h is the fraction of the lost magnetic energy appearing as heat. For $0.68 \le s \le 1$ and $\beta_G \cong 0.22$, we obtain

$$0.58 \le h \le 0.78. \tag{72b}$$

Therefore at least 58% of lost magnetic energy is available for heating.

6. Thermodynamics

We can express many cloud properties as functions of the length of the flux-rope. Setting $l = 2\pi a$ and using the first law of thermodynamics, we get

$$dQ = dW + dU_T \tag{73}$$

where

$$dU_T = N C_V dT,\ dW = P\,dV. \tag{74}$$

where dU_T is the infinitesimal change in internal thermal energy stored in the flux-rope, C_V is the specific heat at constant volume, dW is the infinitesimal work done by the expanding flux-rope, and dQ is the infinitesimal heat added to the volume due to magnetic dissipation as the length of the rope increases by dl. We can write

$$dQ = -h\,dU_m \tag{75}$$

where h is the fraction of magnetic energy dissipated as heat. If the cloud dynamics is governed by the Lorentz self-force, then from (55) and (72), the value of h is expected to lie between 0.58 and 0.78. For now we consider a general range $0 \le h \le 1$. Here h=0 corresponds to adiabatic evolution with no magnetic energy dissipation, while h=1 corresponds to the case when all of the available magnetic energy is dissipated as heat. We also have

$$dU_m(l) = -U_m(l_0)\,l_0\,\frac{dl}{l^2}. \tag{76}$$

where dU_m is the infinitesimal change in magnetic energy stored in the volume of the flux-rope as the length of the rope increases by dl. We can write dW as a function of l as

$$dW(l) = P\,dV = P(l)\,\frac{3V_0}{l_0^3}\,l^2\,dl. \tag{77}$$

Using the ideal gas law $PV = NkT$, where N is total number density of particles present (electrons plus ions) and k is the Boltzmann constant, we can express dU_T as a function of l as

$$dU_T = \left(\frac{C_V}{k}\right)\left(P(l)\,\frac{3V_0}{l_0^3}\,l^2\,dl + \frac{V_0}{l_0^3}\,l^3\,dP(l)\right). \tag{78}$$

Substituting from (75), (76), (77), and (78) into (73) and using $C_P - C_V = k$, we obtain a differential equation for $P(l)$:

$$0 = -hU_m(l_0)\,\frac{l_0^2}{l^2} + \frac{V_0 l^2}{k l_0^2}\left(3C_P P(l) + C_V l\,\frac{d}{dl}P(l)\right). \tag{79}$$

Using $\gamma = C_P/C_V$ and $\beta = 2\mu_0 P/B^2 \cong NkT/U_m$, where P, T, and B are volume averaged values, we get

$$\beta(l_0) = NkT(l_0)/U_m(l_0) = P(l_0)V(l_0)/U_m(l_0) \tag{80}$$

Equation (79) can now be written as

$$\frac{d\left(P(l)/P(l_0)\right)}{d\left(l/l_0\right)} = -3\gamma\,\frac{\left(P(l)/P(l_0)\right)}{\left(l/l_0\right)} + \left(h\,\frac{\gamma-1}{\beta(l_0)}\right)\frac{1}{\left(l/l_0\right)^5} \tag{81}$$

The solution of this differential equation is

$$\begin{aligned}\frac{P(l)}{P(l_0)} &= h\,\frac{1}{\beta(l_0)}\left(\frac{\gamma-1}{3\gamma-4}\right)\left(\frac{l_0^4}{l^4}\right) \\ &\quad + \left[1 - h\,\frac{1}{\beta(l_0)}\left(\frac{\gamma-1}{3\gamma-4}\right)\right]\left(\frac{l_0^{3\gamma}}{l^{3\gamma}}\right),\end{aligned} \tag{82}$$

and using the gas law again we get the temperature:

$$\begin{aligned}\frac{T(l)}{T(l_0)} &= h\,\frac{1}{\beta(l_0)}\left(\frac{\gamma-1}{3\gamma-4}\right)\left(\frac{l_0}{l}\right) \\ &\quad + \left[1 - h\,\frac{1}{\beta(l_0)}\left(\frac{\gamma-1}{3\gamma-4}\right)\right]\left(\frac{l_0^{3(\gamma-1)}}{l^{3(\gamma-1)}}\right).\end{aligned} \tag{83}$$

The corresponding expressions for an adiabatic expansion without any magnetic energy dissipation are obtained by putting h=0 as

$$\frac{P(l)}{P(l_0)} = \left(\frac{l_0^{3\gamma}}{l^{3\gamma}}\right) \tag{84}$$

and

$$\frac{T(l)}{T(l_0)} = \left(\frac{l_0^{3(\gamma-1)}}{l^{3(\gamma-1)}}\right). \tag{85}$$

6.1. Heating the Magnetic Clouds

Adiabatic expansion of model magnetic clouds with $\gamma = 5/3$ leads to cloud temperatures $\cong 3$K at 1 AU, while observed temperatures are $\cong 10^4 - 10^5$ K [*Chen and Garren*, 1993]. Here γ is often made different from the adiabatic value of 5/3 and closer to the isothermal value of 1 to make the models agree with observations. It has been argued that $\gamma \cong 1$ is appropriate, i.e., direct thermal conduction from the Sun might account for the heating. However a typical cloud is at a higher temperature than the photosphere. If the footpoints of a magnetic cloud anchored in the photosphere are roughly at the photospheric temperature (5800 K), then conduction can hardly cause the heating. The second law of thermodynamics forbids heat transfers that lead to a higher temperature in the receiving system than in the source. If one were to say that the conducted heat comes from the hot coronal part of the flux-rope then the problem of the coronal heating mechanism comes to the fore. Since conduction across the field lines is small, we cannot explain the heating by conduction from the external hot corona into the flux-rope. Either something (Alfvén waves, energetic particles?) comes from the Sun along the field lines to heat up the flux-rope or it is the local magnetic energy dissipation that is responsible. There is no widely accepted mechanism for this heating. It is conceivable that some mechanism involving effects of Alfvén wave dissipation or energetic particles might explain the coronal heating. We suggest that the heating is caused by dissipation of local magnetic energy due to small-scale current sheet formation either in field deformations [*Parker*, 1994] or in turbulence [*Vainshtein et al.*, 1993]. Our model does not tell us anything about the mechanism of magnetic energy dissipation; it only tells us how much of the magnetic energy must be lost into other forms as a flux-rope expands, a fraction h of which goes into heating.

From (83) and (85) it is obvious that, for large l and $\gamma > 1$, the first term in the expression for temperature is more important than the adiabatic term. With $\gamma = 5/3$, we get a l^{-1} temperature behavior for large l, instead of l^{-2}, as in the case of adiabatic expansion. Also the temperature at large l depends inversely on the initial plasma beta, which means that a flux-rope with low initial beta would be heated more than one with high initial beta. This dependence on initial plasma beta is not present in the adiabatic case. A log-log plot of $T(l)/T(l_0)$ versus l/l_0 for different initial values of plasma beta $\beta(l_0)$ and for the adiabatic case is shown in Figure 7, where $T(l_0)$ and l_0 are initial temperature and initial length of the flux-rope, respectively.

If the initial beta is less than $(2/3)h$, then the cloud temperature goes through a maximum. The smaller the initial beta, the higher the maximum temperature. The peak in the temperature plot is due to two competing processes: heating due to magnetic energy dissipation and cooling due to

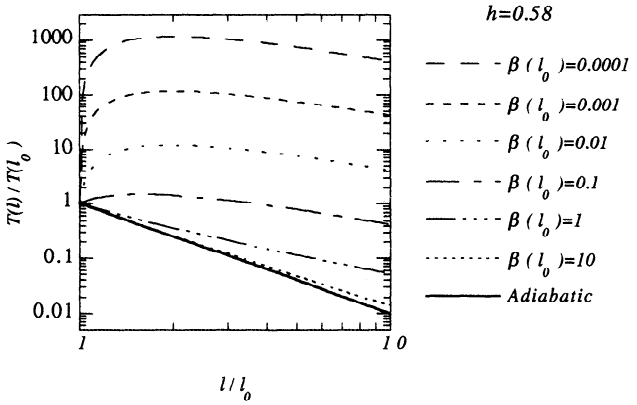

Figure 7. plot of temperature versus length of a flux-rope for various values of starting plasma beta.

expansion. Heating dominates in the early phases of a cloud's evolution. For $\gamma = 5/3$, the maximum in $T/T(l_0)$ is given by the formula

$$\frac{T_{MAX}}{T(l_0)} = \frac{h^2}{3\beta(l_0)[2h - 3\beta(l_0)]}, \tag{86}$$

and the length of the flux-rope for which the maximum in temperature occurs is

$$l_* = l_0\left(2 - \frac{3\beta(l_0)}{h}\right). \tag{87}$$

A log-log plot of $T_{MAX}/T(l_0)$ attained versus the initial plasma beta $\beta(l_0)$ for h=0.58 is shown in Figure 8. If the initial plasma beta is small compared to $(2/3)h$, as is the case with chromospheric and coronal solar flux-ropes, we get simpler formulae:

$$\frac{T_{MAX}}{T(l_0)} \cong \frac{h}{6\beta(l_0)}, \tag{88}$$

and

$$l_* \cong 2l_0 \tag{89}$$

For h=0.58 and $\beta(l_0) = 0.0006$, we see that a flux-rope initially at temperature $T(l_0) \cong 8000$ K can be heated to 161 times its initial temperature, bringing it up to a coronal temperature of 1.3×10^6 K. For h=0.78, the same flux-rope can be heated to 217 times its initial temperature, i.e. to 1.7×10^6 K. While the flux-rope attains its maximum temperature, its length doubles. For a typical flux-rope length of a few hundred thousand kilometers, this means the flux-rope is still within the corona when it attains its maximum temperature.

6.2. Plasma Beta in Magnetic Clouds

The theoretical value for plasma beta as a function of flux-rope length is

$$\beta(l) = \frac{2}{3}h + \left(\beta(l_0) - \frac{2}{3}h\right)\frac{l_0}{l}. \tag{90}$$

Irrespective of its starting value, beta asymptotically approaches a constant value of $(2/3)h$. That is

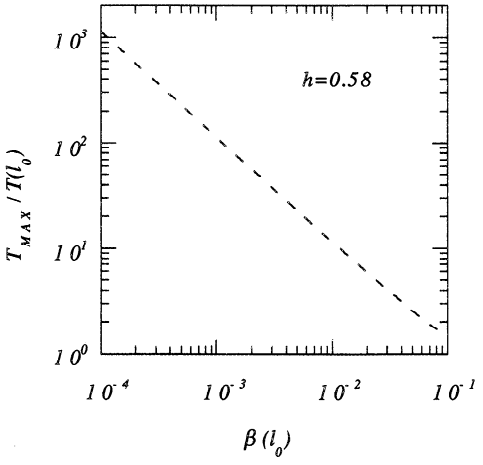

Figure 8. The maximum temperature attained by the flux-rope versus the initial plasma beta.

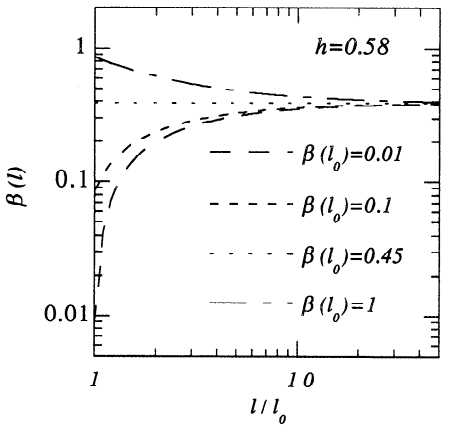

Figure 9. The plasma beta as a function of the length of the flux-rope for various values of initial plasma beta.

$$\lim_{l\to\infty} \beta(l) = \frac{2}{3}h \tag{91}$$

Figure 9 shows theoretical plots of plasma beta versus the length of the flux-rope for various starting values of beta. Most available data for beta in magnetic clouds are for protons only, and the observed proton beta is 0.1-0.2 [*Klein and Burlaga*, 1982]. *Montgomery et al.* [1974] mention that, in low-temperature regions following an interplanetary shock wave associated with the passage of magnetic structures, electron temperatures are 3 to 4 times the proton temperatures. Therefore, the total plasma beta would be between 0.4 and 1. *Burlaga et al.* [1981] find beta values ranging from 0.05 to 1 at different points within a cloud. *Osherovich et al.* [1993b] mention that the ratio of electron temperature to the proton temperature varies across the cloud, remains always larger than 1, and attains values ~10 near the axis of the cloud. For the cloud of March 19,1980, reported by *Osherovich et al.* [1993b] and for an average density of $5\,\mathrm{cm}^{-3}$, the average ratio of temperatures is $T_e/T_p \cong 3.9$, which is consistent with what has been said above. Note that we are only concerned with average total plasma beta in the cloud. Discussion of variations of plasma beta within the cloud and any disparities in electron and proton temperatures are beyond the scope of this paper. However we do want to point out that dissipated magnetic energy goes into heating the magnetic cloud in such a way as to make the average plasma beta in the cloud asymptotically approach a constant value of $(2/3)h$. When the plasma beta in a cloud comes close to this asymptotic value, its speed also approaches a constant. When the cloud speed becomes more or less constant its evolution is similar to the "free self-similar expansion" as described by *Farrugia et al.* [1993] and *Osherovich et al.* [1993c]. This is also consistent with the result of *Osherovich et al.* [1995] that a flux-rope can undergo a "free self-similar expansion" only in the limit of finite beta.

Using the limits on h from relations (72), we get the limits on final beta:

$$0.39 \le \beta_{final} \le 0.52. \tag{92}$$

These limits are consistent with the observations.

6.3. Polytropic Index of a Magnetic Cloud

Consider an observer who follows the particles in an elemental volume of moving fluid and makes repeated

measurements of pressure and number density. A polytropic relationship is said to hold when these variables satisfy an equation of the form $P \sim n^{\Gamma}$. The dimensionless constant Γ is called the polytropic index. In our current-core flux-rope model, we see from (46) and (82) that for $\gamma = 5/3$ and for $l/l_0 >> 1$, pressure and number density are related as

$$P(l) \cong \left(h \frac{2}{3\beta(l_0)} \frac{P(l_0)}{(n(l_0))^{4/3}} \right) n(l)^{4/3}. \quad (93)$$

A polytropic relation indeed holds far from the Sun with $\Gamma = 4/3 \cong 1.33$, which is smaller than the adiabatic value of 5/3. It simply means that due to magnetic heating, the cloud's expansion is not adiabatic. For $l/l_0 >> 1$ the speed of the cloud approaches a constant value. This situation is similar to the self similar radial expansion described by *Low* [1982], who also obtained a polytropic index of 4/3.

Here it is important to mention the results of *Osherovich et al.* [1993b] that the pressure and density obtained at different locations in a magnetic cloud by a passing spacecraft seem to be related by a polytropic kind of relationship with an index of ~0.5 for electrons and ~1.2 for protons. On the face of it the indices obtained are not polytropic since the measurements were not performed successively on the same fluid element, but on different fluid elements with possibly different thermal histories. Osherovich et al. provide a theoretical justification to support their view that these indices are indeed polytropic. Regardless of whether these indices are polytropic or not, they are important observational results which any detailed theory of magnetic clouds must be able to explain.

7. Effects of Expansion

7.1. IMC Boundaries

Burlaga [1988] and *Lepping et al.* [1990] take the axial field component B_z in IMCs to be zero at the boundary corresponding to the first zero of the Bessel function J_0, similar to the current confinement boundary r_0 in the model presented in this paper. Also, no IMCs have features corresponding to higher zeros of J_0, or as *Farrugia et al.* [1991] put it, "no observational magnetic cloud signature has more than one 'cycle' in its components." Observationally, the determination of IMC boundaries is somewhat subjective [*Lepping et al.*, 1990], but we will assume that the uncertainties are not very significant.

7.2. Expansion of the Minor Radius

Since magnetic plus plasma pressure inside IMCs is higher than in the ambient solar wind, it has been argued that excess pressure drives the radial expansion. We find this conclusion unsatisfactory on two counts (1) observations show that the radii of clouds increase approximately linearly with time [*Bothmer and Schwenn*, 1994], i.e. the radial expansion velocities are approximately constant. Any excess pressure driving the expansion would instead give rise to an acceleration which would cause the radial expansion velocity to increase with time. (2) It does not take into account the radial component of magnetic tension in the helically curved field lines. In fact, in the case of the usual force-free model of a magnetic cloud, the centrifugal force due to the magnetic pressure is exactly balanced by the centripetal force due to magnetic tension, so that in this case, magnetic pressure does not play a role in the expansion of the magnetic cloud.

In our current-core flux-ropes, the minor radius (which is the same as the current-confinement radius) is quite insensitive to the conditions in the external environment. Changes in the minor radius take place mainly due to changes in the internal magnetic configuration. Conservation of magnetic helicity and axial flux dictate the form of the radial expansion. If the length of a flux-rope increases, conservation of helicity and axial flux can be achieved only if the flux-rope also expands laterally. For the toroidal flux-rope considered in this paper, the same effect is obtained if one uses conservation of axial and azimuthal flux.

This conclusion can be made more concrete by using (40) to see that the aspect ratio of the cloud must remain constant, i.e.,

$$l/r_0(l) = \text{const.} \quad (94)$$

Therefore the length and minor radius of a cloud moving at constant speed both evolve linearly with time. This result is in agreement with observations of *Bothmer and Schwenn* [1994] and theoretical results of *Chen and Garren* [1993].

7.3. Slope of the Plasma Velocity Profile in Clouds

The measured plasma velocity in IMCs shows a characteristic profile, with the leading edge usually moving faster and the trailing edge usually moving slower than the ambient solar wind. Between these two extremes, the speed decreases with a constant slope (see Figure 10). Sometimes shocks affect the velocity profile, but the negative slope is usually unmistakable. It is due to the expansion of the cloud [*Farrugia et al.*, 1993]. To describe it, we assume a toroidally shaped cloud with major radius a, minor radius r_0, length $l = 2\pi a$, and distance from the Sun $d = 2a$ (see Figure 2). If the center of the cloud moves at a constant speed V_c, then the cloud expansion speed V_{exp} is given as

$$V_{\text{exp}} = \frac{dr_0}{dt} = \frac{r_0(l_0)}{l_0}\frac{dl}{dt} = \frac{r_0(l_0)}{l_0} 2\pi \frac{da}{dt} = \frac{r_0(l_0)}{l_0}\pi V_c, \quad (95)$$

where we have used (40) for radius as a function of length, and we have taken the cloud speed V_c as the rate of change of the distance $d = 2a$ from the Sun. Then, if V_c is constant in time, V_{exp} also remains constant. We can also write

$$V_{\text{exp}} = \frac{r_0(l_0)}{l_0}\pi V_c = \frac{r_0(l)}{l}\pi V_c = \frac{r_0(d)}{d} V_c. \quad (96)$$

Assuming that during the cloud's passage across a spacecraft, its speed V_c and therefore V_{exp}, do not vary, then the leading edge would appear to move at $V_c + V_{\text{exp}}$ while the trailing edge would appear to move at $V_c - V_{\text{exp}}$. This gives the slope of the velocity profile as

$$\text{slope} = \frac{\left(V_c + V_{\text{exp}}\right) - \left(V_c - V_{\text{exp}}\right)}{\Delta t} = \frac{2V_{\text{exp}}}{\Delta t}, \quad (97)$$

where Δt is the time interval of passage. It can readily be shown that the slope of the velocity profile satisfies the following relation:

$$\text{slope} = \frac{V_c^2}{d}\left(1 - \left(\frac{r_0}{d}\right)^2\right), \quad (98)$$

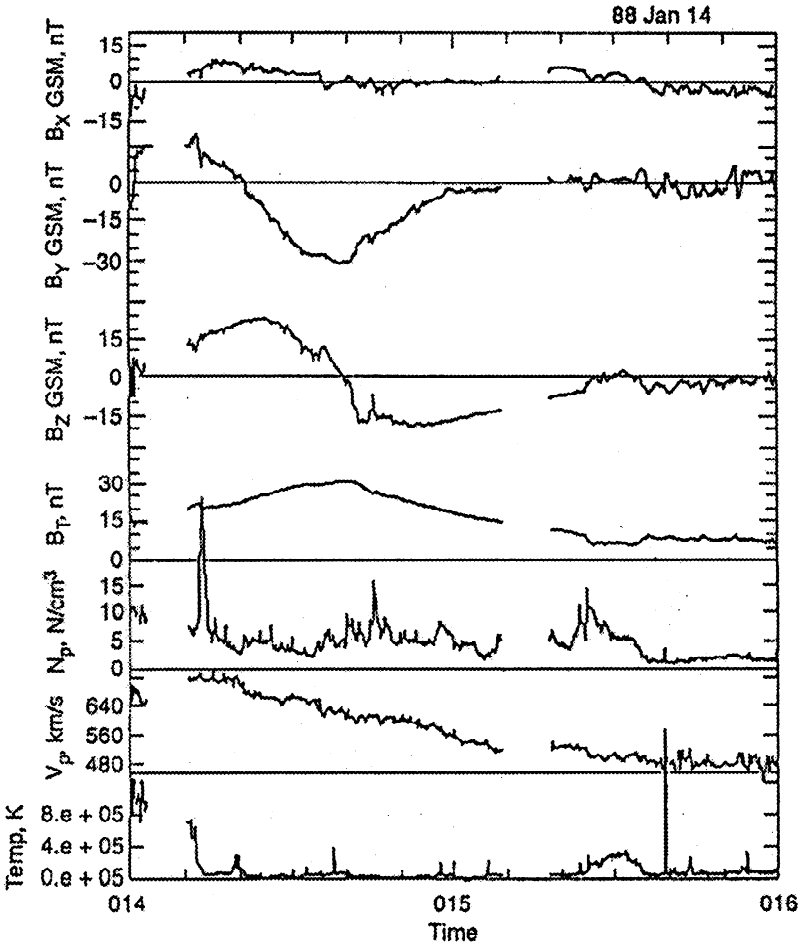

Figure 10. IMP-8 spacecraft data for the magnetic cloud of January 14, 1988. The cloud passed the spacecraft between 0400 UT on the 14th and 1200 UT on the 15th. Note the smooth variation of the magnetic field and the asymmetry of the magnetic strength profile. The slope of the proton velocity is approximately constant through the cloud.

where all the quantities are expressed at a time when cloud center is passing the spacecraft. The factor in the brackets is close to unity (at $d = 1$ AU and for $r_0 = 0.14$ AU, $1-(r_0/d)^2 \cong 0.98$). Therefore we get

$$\text{slope} \cong V_c^2/d. \tag{99}$$

All the quantities in (99) can be calculated from the available cloud data, including the slope of the measured velocity profile, the speed of the center of the cloud and the distance of the cloud from the Sun. As an example consider the cloud of January 13, 1988 (Figure 10). For this cloud, $V_c \cong 638\ \text{km s}^{-1}$, $d = 1$ AU, and the measured value of the slope $\cong 2.83\ \text{m s}^{-2}$, while the theoretical value of the slope is $V_c^2/d \cong 2.71\ \text{m s}^{-2}$.

Figure 11 shows a plot of the theoretical slope V_c^2/d versus the measured slope of the velocity profile for 24 clouds, where V_c is the speed of the center of the cloud. A straight line fit gives

$$V_c^2/d = 1.04 \times \text{measured slope}, \tag{100}$$

which shows excellent agreement between theory and observations.

7.4. Asymmetry of the Magnetic Field Strength Profile

In cloud data where the magnetic field strength profile is not corrupted by the presence of shocks or interaction regions, one finds that the maximum magnetic field strength appears to be displaced toward the leading end of the cloud (see Figure

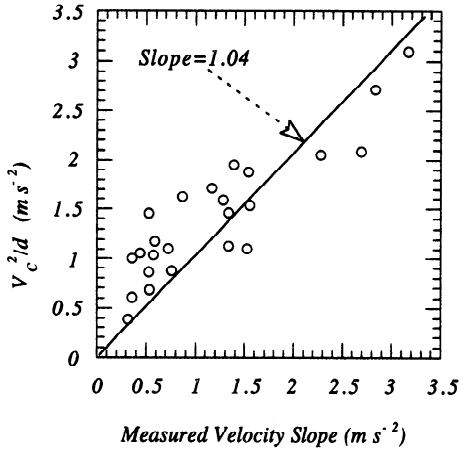

Figure 11. The theoretical velocity slope within the magnetic cloud versus the measured velocity slope.

10). This asymmetry is due to expansion of the clouds [*Farrugia et al.*, 1991] since the time that it takes for the center of the cloud to arrive at the spacecraft after the front edge has passed will be shorter than the time taken by the trailing end to arrive after the center has passed, due to continual expansion of the cloud. We can obtain a measure of the asymmetry by taking the ratio of these two time intervals,

$$\text{asymmetry} = \frac{\text{time interval between front and center}}{\text{time interval between center and rear}} = \frac{\Delta t_c}{\Delta t - \Delta t_c} = \frac{V_c - V_{\exp}}{V_c + V_{\exp}} = \frac{1 - r_0/d}{1 + r_0/d} \quad (101)$$

where Δt_c is the time interval between arrival of the leading edge and the center of the cloud. As an example consider the cloud of January 14, 1988 (Figure 10). For this cloud, $r_0 \cong 0.22$ AU and $d = 1$AU. Therefore the theoretical asymmetry is 0.64, while the measured asymmetry is 0.65.

7.5. Effect of Variation in Direction of Motion of Clouds

In deriving the formula for the slope of the velocity profile within a cloud, we implicitly assumed that the distance from the Sun of the observed portion was equal to twice the major radius of the torus. However this will happen only in the case of a head-on encounter. In the general case, if we know the ecliptic latitude λ and ecliptic longitude ϕ (measured counterclockwise with $\phi = 0$ direction pointing toward the Sun) of the axis of the cloud at the point of encounter, then the relation between the major diameter $2a$ of the toroidal cloud and the distance d from the Sun at the point of encounter is

$$d = 2a|f(\lambda,\phi)|, \quad (102)$$

where

$$f(\lambda,\phi) = \sqrt{1 - \cos^2(\lambda)\cos^2(\phi)}. \quad (103)$$

A head-on encounter corresponds to either $\cos(\phi) \cong 0$ or $\cos(\lambda) \cong 0$, and in such cases $f(\lambda,\phi)$ is a very slowly varying function of λ and ϕ, and it remains close to 1. From a study of 18 clouds at 1 AU, *Lepping et al.* [1990] found that, on average, the direction of a cloud's axis satisfied $|\lambda| \cong 42^0$, $\lambda \cong -15^0$, and $\phi \cong 102^0$. Substituting these values into the expression for $f(\lambda,\phi)$, we get $f(42^0,102^0) \cong 0.988$ and $f(15^0,102^0) \cong 0.980$. We conclude that, on average, the formula $d \cong 2a$ holds within 2% accuracy for the clouds reported. In the following we use this formula without the correction factor $f(\lambda,\phi)$.

8. Comparison with Observations

In this section we compare our model with published IMC data. The data used here have been taken from *Burlaga* [1988], *Burlaga et al.* [1981, 1982], *Burlaga and Behannon* [1987], *Burlaga and Behannon* [1982], *Klein and Burlaga* [1982], *Lepping et al.* [1990, 1991], *Marubashi* [1986], *Zhang and Burlaga* [1988], *Farrugia et al.* [1991, 1993], *Zhang* [1991], *Montgomery et al.* [1974], *Gosling et al.* [1987], *Bothmer and Schwenn* [1991] and *Vandas et al.* [1991, 1993].

To compare with the observations, we have used the following scaling laws from our model (see (38), (46), (40) and (83)):

Magnetic field strength

$$B_0 \sim \frac{1}{d^2}, \quad (104)$$

Number density

$$n \sim \frac{1}{d^3}, \quad (105)$$

Radius

$$r_0 \sim d, \quad (106)$$

Temperature

$$T \sim \frac{1}{d} + O\left(\frac{1}{d^2}\right), \quad (107)$$

where d is the distance from the Sun and the length l of the flux-rope is related to d as $l = \pi d$. We have also used $\gamma = 5/3$. In our model, temperature is not a power law function of d, but at the distances where cloud data are available, the first term in the expression for temperature (see (83) and (107)), dominates. Therefore, for purposes of comparison with data, our theoretical model predicts an inverse distance dependence for the temperature.

Table 1 shows the fit parameters for the data obtained from a power law fit and also from a fit using the theoretical model. It

Table 1. Verification of Scaling Laws from Observations

Observables	Power Law Fit	Fit based on the theoretical model	Total Number of Clouds	Clouds at $d < 1$AU	Clouds at $d > 1$AU
B_0, nT	$18.4/d^{1.8}$	$18.8/d^2$	52	3	9
n, cm^{-3}	$7.2/d^{2.8}$	$5.8/d^3$	25	3	4
r_0, AU	$0.148\,d^{0.97}$	$0.155\,d$	34	3	4
$T_p, 10^4$ K	$3.4/d^{0.7}$	$3.6/d$	18	3	2

Fit parameters for the strength of the axial magnetic field B_0, average proton number density n, radius r_0 of the cloud, and proton temperature T_p. d is the distance from the Sun. From the power law fit, two parameters, the multiplicative constant and the exponent, were determined. In the case of fits based on the theoretical model, the exponent was taken to be as given by the theory, and the multiplicative constant was determined from the fits.

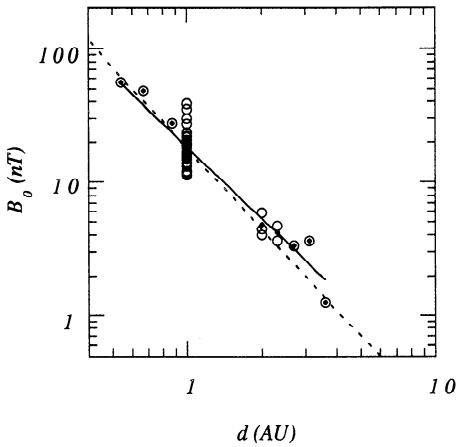

Figure 12. The strength of the magnetic field B_0 at the axis of a magnetic cloud versus the distance from the Sun.

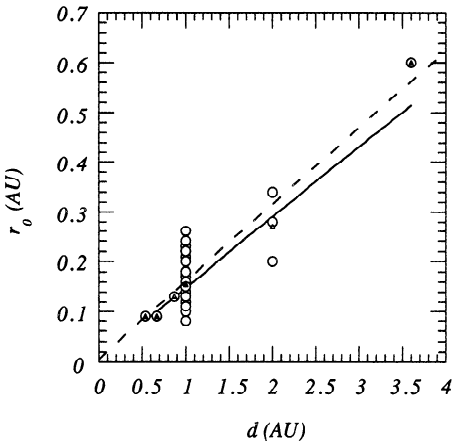

Figure 14. The radius of the magnetic cloud versus the distance from the Sun.

also shows the total number of clouds used. In the case of power law fit, the multiplicative constant and the exponent were the two parameters determined from the fit. In the case of the "theoretical" fit the exponent was taken to be given by the theoretical scaling laws (see (104) through (107)), and only the multiplicative constant was determined from the fit. We see that the power law fit gives exponents that are close to the exponents expected from the model.

Figures 12 through 15 show plots of axial magnetic field strength, proton number density, radius, and temperature as functions of distance d from the Sun. Empty circles represent individual data points, while solid triangles represent mean values obtained at each value of d. In each figure the solid line shows the power law fit to the data, and the dashed line shows the fit based on the theoretical model as given in Table 1.

As most clouds were observed at 1 AU, statistics for data at that d value are better than for the others. However, the fits listed in Table 1 and the figures show that the data from 0.3 to 4 AU are in good agreement with the model. More data on clouds at different distances from the Sun could help to refine the comparisons. Note that the fitted parameters obtained are for an average IMC, and individual clouds may show substantial variations. The variability in the observed clouds is mainly due the variability in their parent structures on the Sun (usually a solar filament). The differences in the parent structure can, in turn, be due to differences in strength of magnetic field, length, diameter, height above the solar surface before ejection, footpoint separation. If injection of helicity triggers the ejection of the parent structure [*Rust and Kumar*, 1994b] , then differences in rate of helicity injection (or for that matter, differences in any triggering mechanism) would cause differences in the dynamical properties. However the exchange of magnetic helicity (or any magnetic quantity) with the Sun stops when the speed of the cloud becomes larger than the speed of the Alfvén waves along the field lines.

9. Conclusions

We have presented a model for interplanetary magnetic clouds as flux-ropes whose properties are determined intrinsically by their initial values. The model explains clouds' average magnetic and thermodynamic properties, as well as their dimensional variations as a function of distance from the Sun. With the assumption that magnetic clouds can be approximated as large-aspect-ratio tori which remain connected to the Sun, all quantities involved become functions of the distance of the observed part of the cloud from the Sun. This makes it possible to compare the predictions of the model with data obtained from spacecraft located at various

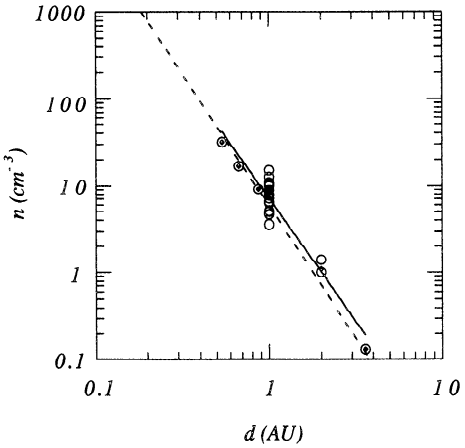

Figure 13. The average proton number density within magnetic clouds versus the distance from the Sun.

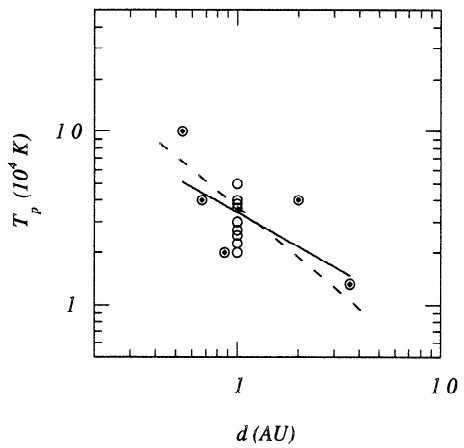

Figure 15. The average proton temperature in the clouds versus the distance from the Sun.

distances from the Sun. The results of comparisons between the model and data on the magnetic field strength, density, radius, and cloud temperature as functions of distance from the Sun, are given in Table 1. Other observables considered were asymmetry of the magnetic field strength profile, slope of the plasma velocity profile inside clouds, and the plasma beta.

According to this model, a cloud's evolution is constrained by conservation of three quantities: magnetic flux, magnetic helicity and mass. Dimensionally, magnetic helicity is proportional to magnetic energy times a length scale, i.e. $H_m \propto (\text{length scale}) \times U_m$. Therefore, generally speaking, under the constraint of conservation of magnetic helicity, the magnetic energy stored in magnetized plasmas should decrease with expansion. One expects that a part of this lost magnetic energy would go into heating the plasma. Therefore, conservation of magnetic helicity implies that expanding magnetized plasmas could be heated by magnetic energy dissipation. We believe that this idea can be applied not only to interplanetary magnetic clouds but also to various astrophysical phenomena, such as stellar and galactic winds, stellar coronae, nebulae, and supernova remnants.

One of the more important results of our model, derived from application of the above idea, is the explanation of the high temperatures in magnetic clouds. Helicity conservation leads to a simple expression for the decrease in magnetic energy of a flux-rope as a function of its length (see (28)). Therefore, during expansion, some magnetic energy stored in the flux-rope is continuously being made available for conversion into other forms. Assuming that the dynamics of the clouds is governed by magnetic forces, some of this decrease in the magnetic energy appears as bulk kinetic energy and some acts against solar gravity. Even after accounting for these losses, we found that 58% to 78% of the available magnetic energy remains unaccounted for. Most likely, it is converted into heat in small-scale turbulence, while the large-scale structure remains intact. As a flux-rope expands, and before it leaves the corona, its temperature increases sharply to coronal values. The maximum temperature achieved depends inversely upon the initial plasma beta. Above the corona, cooling by expansion of the entrained plasma begins to dominate, but the derived cloud temperature at 1 AU remains large enough to be in agreement with the observations.

The mechanisms for heating the solar corona and solar wind are not exactly known, but it is widely believed that the energy is supplied by magnetic fields. Magnetic helicity conservation has been used to determine the heating rates in some coronal heating models [*Heyvaerts and Priest*, 1984]. They assumed that the buildup of free magnetic energy and helicity in coronal loops is due to photospheric motions. This buildup in general led to a nonlinear force-free magnetic structure. Then the excess magnetic energy above the corresponding Taylor relaxed state [*Taylor*, 1974, 1986] was assumed to be released in a fast reconnection process. Magnetic helicity was assumed to remain constant during the relaxation process.

We briefly examined the dynamics of clouds with the encouraging result that low-lying flux-ropes, i.e. those starting at only 0.01 solar radii above the surface, accelerate more rapidly and achieve a higher peak velocity than those at 0.10 solar radii. This result is in qualitative agreement with observations of coronal mass ejections.

Interplanetary magnetic clouds originate on the Sun, and most, if not all of them are associated with solar filament eruptions [*Rust*, 1994]. Parameters determined from the magnetic cloud data, if extended back to the Sun may tell us more about these solar structures. Since solar filaments and IMCs both exhibit flux-rope structure, it should be possible to strengthen the connection between them. It is also possible that helicity conservation can be usefully applied to describe the physics of other helical flux-ropes such as those in the photosphere and in Venus' ionosphere.

Acknowledgements. Ashok Kumar's work was supported by The Johns Hopkins University Applied Physics Laboratory Graduate Fellowship Program. David M. Rust's work was supported by the NASA Solar Physics Program and by the National Science Foundation under grant DPP-9119807.

The Editor thanks M.L.Goldstein and another referee for their assistance in evaluating this paper.

References

Anzer, U., Can coronal loop transients be driven magnetically?, *Sol. Phys.*, *57*, 111, 1978.

Batchelor, G.K., *Theory of Homogeneous Turbulence*, 121 pp., Cambridge Univ. Press, New York, 1970.

Berger, M.A., Rigorous new limits on magnetic helicity dissipation in the solar corona, *Geophys. Astrophys. Fluid Dyn.*, *30*, 79-104, 1984.

Berger, M. A. and G. B.Field, The topological properties of magnetic helicity, *J. Fluid Mech.*, *147*, 133, 1984.

Bothmer, V., and R. Schwenn, Magnetic cloud observations by the Helios spacecraft, in *Solar Wind Seven*, edited by R. Schwenn and E. Marsch, 599 pp., Pergamon, Oxford, 1991.

Bothmer, V., and R. Schwenn, Eruptive prominences as sources of magnetic clouds in the solar wind, *Space Sci. Rev.*, *70*, 215, 1994.

Burlaga, L.F., Magnetic clouds and force-free fields with constant alpha, *J. Geophys. Res.*, *93*, 7217, 1988.

Burlaga, L. F., and K. W. Behannon, Magnetic clouds: Voyager observations between 2 and 4 AU, *Sol. Phys.*, *81*, 181, 1982.

Burlaga, L. F., and K. W. Behannon, Compound streams, magnetic clouds and major geomagnetic storms, *J. Geophys. Res.*, *92*, 5725, 1987.

Burlaga, L., E. Sittler, F. Mariani, and R. Schwenn, Magnetic loop behind an interplanetary shock: Voyager, Helios and IMP 8 observations, *J. Geophys. Res.*, *86*, 6673, 1981.

Burlaga, L. F., L. Klein, N. R. Sheeley Jr., D. J. Michels, R. A. Howard, M. J. Koomen, R. Schwenn, and H. Rosenbauer, A magnetic cloud and a coronal mass ejection, *Geophys. Res. Lett.*, *9*, 1317, 1982.

Burlaga, L. F., L. W. Klein, R. P. Lepping, and K. W. Behannon, Large scale interplanetary magnetic fields: Voyager1 and 2 observations between 1 AU and 9.5 AU, *J. Geophys. Res.*, *89*, 10659, 1984.

Burlaga, L. F., F. B. McDonald, M. L. Goldstein, and A. J. Lazarus, Cosmic ray modulation and turbulent interaction region near 11 AU, *J. Geophys. Res.*, *90*, 12027, 1985.

Burlaga, L. F., R. P. Lepping, and J. A. Jones, Global configuration of a magnetic cloud, in *Physics of Magnetic Flux Ropes, Geophys. Monogr. Ser.*, vol. 58, edited by C. T. Russell, E. R. Priest and L. C. Lee, pp. 373-378, AGU, Washington, D. C., 1990.

Chen, J., Effects of toroidal forces in current loops embedded in a background plasma, *Astrophys. J.*, *338*, 453, 1989.

Chen, J., Dynamics, catastrophe and magnetic energy release of toroidal solar current loops, in *Physics of Magnetic Flux Ropes, Geophys. Monogr. Ser.*, vol. 58, edited by C.T. Russell, E.R. Priest and L.C. Lee, pp.269-278, AGU, Washington, DC, 1990.

Chen, J., and D. A. Garren, Interplanetary magnetic clouds: Topology and driving mechanism, *Geophys. Res. Lett.*, *20*, 2319, 1993.

Elsasser, W. M., Hydromagnetic dynamo theory, *Rev. Mod. Phys.*, *28*, 135, 1956.

Farrugia, C. J., L. F. Burlaga, V. A. Osherovich, and R. P. Lepping, A comparative study of dynamically expanding force-free constant-alpha magnetic configurations with applications to magnetic clouds, in *Solar Wind Seven*, edited by R. Schwenn and E. Marsch, pp. 611-614, Pergamon, New York, 1991.

Farrugia, C. J., L. F. Burlaga, V. A. Osherovich, I. G. Richardson, M. P. Freeman, R. P. Lepping, and A. J. Lazarus, A study of an expanding interplanetary magnetic cloud and its interaction with the Earth's magnetosphere: The interplanetary aspect, *J. Geophys. Res.*, *98*,(A5), 7621, 1993.

Feynman, J., and A. J. Hundhausen, Coronal mass ejections and major solar flares: The great active center of march 1989, *J. Geophys. Res., 99*, 8451, 1994.

Finn, J. M. and T. M. Antonsen, Magnetic helicity: What is it and what is it good for?, *Comments Plasma Phys. Controlled Fusion, 9*(3), 111, 1985.

Frisch, U., A. Pouquet, J. Leorat, and A. Mazure, Possibility of an inverse cascade of magnetic helicity in magnetohydrodynamic turbulence, *J. Fluid Mech., 68*, 769, 1975.

Garren, D.A., and J. Chen, Lorentz self-forces on curved current loops, *Phys. Plasmas, 1* (10), 3425, 1994.

Ghosh, S., W. T. Stribling, M. L. Goldstein, and W. H. Matthaeus, The evolution of magnetic helicity in compressible magnetohydrodynamics with a mean magnetic field, in *Space Plasmas: Coupling Between Small and Medium Scale Processes, Geophys. Monogr. ser.* vol. 86, edited by M. Ashour-Abdalla, T. Chang, and P. Dusenbery, pp. 1-5, AGU, Washington, D. C., 1995.

Goldstein, H., On the field configuration in magnetic clouds, in *Solar Wind Five*, NASA Conf. Publ., CP-2280, 731-733, 1983.

Gosling, J. T., D. N. Baker, S. J. Bame, W. C. Feldman, and R. D. Zwickl, Bidirectional solar wind electron heat flux events, *J. Geophys. Res., 92*(A8), 8519, 1987.

Heyvaerts, J. and E. R. Priest, Coronal heating by reconnection in DC current systems: A theory based on Taylor's hypothesis, *Astron. Astrophys., 137*, 63, 1984.

Hundhausen, A.J., The origin and propagation of coronal mass ejections, *Solar Wind Six, Tech. Note NCAR/TN Proc., 306*, 181, Natl. Cent. for Atmos. Res., Boulder, Colo., 1988.

Ivanov, K. G., and A. F. Harshiladze, Interplanetary hydromagnetic clouds as flare generated spheromacs, *Sol. Phys., 98*, 379, 1985.

Ivanov, K. G., A. F. Harshiladze, E. G. Eroshenko,. and V. A. Styazhkin, Configuration, structure, and dynamics of magnetic clouds from solar flares in light of measurements on board Vega 1 and Vega 2 in January-February 1986, *Sol. Phys., 120*, 407, 1989.

Jensen, T. H., and M. S. Chu, Current drive and helicity injection, *Phys. Fluids, 27*, 2881, 1984.

Klein, L. W., and L. F. Burlaga, Interplanetary magnetic clouds at 1 AU, *J. Geophys. Res., 87*, 613, 1982.

Kolmogorov, A. N., Local properties of turbulence in incompressible viscous fluids with very large Reynolds numbers, *Dokl. Akad. Nauk SSSR, 30*, 299, 1941.

Kolmogorov, A. N., A refinement of previous hypotheses concerning the local structure of turbulence in a viscous incompressible fluid at high Reynolds number, *J. Fluid Mech., 13*, 82, 1962.

Kraichnan, R. H., Inertial range spectrum in hydromagnetic turbulence, *Phys. Fluids, 8*, 1385, 1965.

Lamb, H., *Hydrodynamics*, pp. 236-241, Reprint of 1932 ed., Cambridge Univ. Press, New York, 1993.

Landau, L. D., and E. M. Lifshitz, *Electrodynamics of Continuous Media*, p. 139, Pergamon, New York, 1960.

Lepping, R. P., J. A. Jones, and L. F. Burlaga, Magnetic field structure of interplanetary magnetic clouds at 1 AU, *J. Geophys. Res., 95*(A8), 11957, 1990.

Lepping, R. P., L. F. Burlaga, B. T. Tsurutani, K. W. Ogilive, A. J. Lazarus, D. S. Evans, and L. W. Klein, The interaction of a very large interplanetary magnetic cloud with the magnetosphere and with cosmic rays, *J. Geophys. Res., 96*, 9425, 1991.

Low, B. C., Self-similar magnetohydrodynamics. I - The gamma = 4/3 polytrope and the coronal transient, *Astrophys. J. 254*, 796, 1982.

Lundquist, S., Magnetohydrostatic fields, *Ark. Fys., 2*, 361, 1950.

Marubashi, K., Structure of the interplanetary magnetic clouds and their solar origins, *Adv. Space Res., 6*(6), 335-338, 1986.

Matthaeus, W. H. and M. L. Goldstein, Measurement of the rugged invariants of magnetohydrodynamic turbulence in the solar wind, *J. Geophys. Res., 87*, 6011, 1982.

Matthaeus, W. H. and D. Montgomery, Selective decay hypothesis at high mechanical and magnetic Reynolds numbers, *Ann. N. Y. Acad. Sci., 357*, 203-222, 1980.

Matthaeus, W. H., M. L. Goldstein, and C. Smith, Evaluation of magnetic helicity in homogeneous turbulence, *Phys. Rev. Lett., 48*, 1256, 1982.

Miller, G., and L. Turner, Force-free equilibria in toroidal geometry, *Phys. Fluids 24*(2), 363, 1981.

Montgomery, M. D., J. R. Asbridge, S. J. Bame, and W. C. Feldman, Solar wind electron temperature depressions following some interplanetary shock waves: evidence for magnetic merging?, *J. Geophys. Res., 79*(22), 3103, 1974.

Moore, R. L., Evidence that magnetic energy shedding in solar filament eruptions is the driver in accompanying flares and coronal mass ejections, *Astrophys. J., 324*, 1132, 1988.

Mouschovias, T. C. and A. I. Poland, Expansion and broadening of coronal loop transients: a theoretical explanation, *The Astrophys. J., 220*, 675, 1978.

Osherovich, V. A., C. J. Farrugia, and L. F. Burlaga, The non linear evolution of magnetic flux-ropes, 1, Low-beta limit, *J. Geophys. Res., 98*, 13,225, 1993a.

Osherovich, V. A., C. J. Farrugia, L. F. Burlaga, R. P. Lepping, J. Fainberg, and R. G. Stone, Polytropic relationship in interplanetary magnetic clouds, *J. Geophys. Res., 98*, 15,331, 1993b.

Osherovich, V. A., C. J. Farrugia, and L. F. Burlaga, Dynamics of aging magnetic clouds, *Adv. Space Res., V. 13*(6), 57, 1993c.

Osherovich, V. A., C. J. Farrugia, and L. F. Burlaga, Nonlinear evolution of magnetic flux-ropes, 2, Finite beta plasma, *J. Geophys. Res., 100*, 12307, 1995.

Parker, E. N., *Spontaneous Current Sheets in Magnetic Fields*, p. 15, Oxford Univ. Press, New York, 1994.

Rust, D. M., Spawning and shedding of helical magnetic fields in the solar atmosphere, *Geophys. Res. Lett., 21*, 241, 1994.

Rust, D. M. and A. Kumar, Helical magnetic fields in filaments, *Sol. Phys., 155*, 69, 1994a.

Rust, D. M. and A. Kumar, Helicity charging and eruption of magnetic flux from the sun, in *Proc. of the Third SOHO Workshop-Solar Dynamic Phenomena and Solar Wind Consequences*, p. 39, 1994b.

Ruzmaikin, A., P. Akhmetiev, Topological invariants of magnetic fields, and the effect of reconnections, *Phys. Plasmas, 1*(2), 331, 1994.

Shafranov, V. D., Plasma equilibrium in a magnetic field, *Rev. Plasma Phys., 2* 113, 1966.

Stribling, T., W. H. Matthaeus, and S. Ghosh, Nonlinear decay of magnetic helicity in magnetohydrodynamic turbulence with a mean magnetic field, *J. Geophys. Res., 99*, 2567, 1994.

Sturrock, P. A., *Plasma Physics*, p. 176, Cambridge Univ. Press, New York, 1994.

Taylor, J. B., Relaxation of toroidal plasma and generation of reverse magnetic fields, *Phys. Rev. Lett., 33*, 1139, 1974.

Taylor, J. B., Relaxation and magnetic reconnection in plasmas, *Rev. Mod. Phys., 58*(3), 741, 1986.

Vainshtein, S. I., A. M. Bykov, and I. N. Toptygin, Dynamics of the magnetic field: Rapid dissipation, in *Turbulence, Current Sheets and Shocks in Cosmic Plasma*, pp. 100, Gordon and BreachNewark, N.J., 1993.

Vandas, M., S. Fisher, P. Pelant, and A. Geranios, Magnetic clouds: Comparison between spacecraft measurements and theoretical magnetic force-free solutions, in *Solar Wind Seven*, edited by R. Schwenn and E. Marsch, 671-674 pp., Pergamon, 1991.

Vandas, M., S. Fisher, P. Pelant, and A. Geranios, Spheroidal models of magnetic clouds and their comparison with spacecraft measurements, *J. Geophys. Res., 98*, 11467, 1993.

Wilson, R. M. and E. Hildner, Are interplanetary magnetic clouds manifestations of coronal transients at 1 AU?, *Sol. Phys., 91*, 168, 1984.

Wilson, R. M. and E. Hildner, On the association of magnetic clouds with disappearing filaments, *J. Geophys. Res., 91*(A5), 5867, 1986.

Woltjer, L., A theorem on force-free magnetic fields, *Proc. Natl. Acad. Sci. USA, 44*, 489, 1958.

Zhang, G. L., Intense magnetic clouds and their interactions with ambient solar wind streams, in *Solar Wind Seven*, edited by R. Schwenn and E. Marsch, 689-692 pp., Pergamon, New York, 1991.

Zhang, G. and L. F. Burlaga, Magnetic clouds, geomagnetic disturbances and cosmic ray decreases, *J. Geophys. Res., 93*, 2511, 1988.

A. Kumar, Department of Physics & Astronomy, Johns Hopkins University, Baltimore, MD 21218. (e-mail: ashok_kumar@jhuapl.edu)

D. M. Rust, Applied Physics Laboratory, Johns Hopkins University, Laurel, MD 20723. (e-mail: david_rust@jhuapl.edu)

(Received June 2, 1995; revised February 15, 1996; accepted February 15, 1996.)